SIMTRAN-E: A SIMULATE-E to RETRAN-02 Datalink

NP-5509-CCM
Research Projects 1761-14, -17

Computer Code Manual, December 1987

Prepared by

EI INTERNATIONAL, INC.
Post Office Box 736
Idaho Falls, Idaho 83402

Principal Investigators
J. A. McClure
G. C. Gose

Prepared for

Electric Power Research Institute
3412 Hillview Avenue
Palo Alto, California 94304

EPRI Project Manager
L. J. Agee

Nuclear Reload Management Program
Nuclear Power Division

THE COMPARISON OF ONE-DIMENSIONAL AND POINT KINETICS FOR VARIOUS LWR TRANSIENTS

J.A. NASEK, C. LIN
ELECTRIC POWER RESEARCH INSTITUTE

G.C. GOSE, J.A. McCLURE
ENERGY INCORPORATED

Y. MATSUI
NIPPON ENERGY INCORPORATED

Project No. 82-219

INTRODUCTION

The need for a one-dimensional kinetics capability has been demonstrated for pressurization transients in Boiling Water Reactors (BWR). In particular, the three turbine trip tests at the Peach Bottom 2 plant (1, 2) demonstrated a considerable change in the axial flux distribution during the transient. There is a strong and nonlinear interaction between the moderator density and the reactivity. Because of this it is important to be able to calculate the change in the axial flux distribution during the transient.

A one-dimensional kinetics capability based on the factorization method (3) has been implemented in RETRAN-02 (4). The factorization method assumes that the flux can be represented as the product of a rapidly varying time function and a slowly varying shape function. RETRAN allows the user to control the frequency in which the shape function is calculated. An approximation to the classic point kinetics models can be obtained by using the initial shape function throughout the entire transient.

The differential equation for the time function is quite similar to the classic point kinetics equation. The parameters that are varying in the equation are computed from the two group cross-section set and reflect the RETRAN thermal-hydraulic conditions. Thus in RETRAN, the point kinetics calculation can be performed with two different approaches.

The first is to use the traditional point kinetics equations and the second is to do an infinite time step for the shape function in the one-dimensional calculation. By not changing the shape function, the latter is equivalent to doing point kinetics; however, by using the one-dimensional cross-sections rather than the point kinetics reactivity curves.

An important input to the kinetics calculation are the cross-sections for one-

dimensional kinetics and the reactivity and scram curves for point kinetics. These cross-sections must come from some physics (i.e., fuel management) code. In general, BWR utilities use the SIMULATE-E (5) and PWR utilities either use the NODEP-2 (6) or SIMULATE-E code for fuel management. These two codes are both three-dimensional nodal codes which have the required cross-sections available in three dimensions. The SIMTRAN-E (7) and NODETRAN (8) computer codes were developed to obtain two-group, one-dimensional cross-sections and consistent point kinetics parameters from the upstream physics codes.

The object of this paper is to compare the results from the three kinetics options: 1) point kinetics; 2) point kinetics by not changing the shape function; and 3) one-dimensional kinetics for various transients on both BWRs and PWRs. A systematic evaluation of the one-dimensional kinetics calculation and its alternatives is performed to determine the status of these models and to identify additional development work. In addition, for PWRs, the NODEP-2 - NODETRAN and SIMULATE - SIMTRAN paths for calculating kinetics parameters are compared. This type of comparison has not been performed before and is needed to properly evaluate the RASP methodology of which these codes are a part. It should be noted that RASP is in its early pre-release stage and this is the first serious attempt to examine the consistency between these two similar but different methods of generating physics parameters for RETRAN.

BWR ANALYSIS

The first set of calculations were performed on a typical BWR. Four transients were selected to evaluate the capabilities of the various kinetics options. They are:

1. Turbine trip without bypass and without scram (TTWOB ATWS) from 100% power and 100% flow.

2. Full rod insertion scram from 100% power and 100% flow.

3. A Turbine trip with bypass from 47.4% power and 98.8% flow with a delayed scram (TT1).

4. Turbine trip with bypass from 61.6% power and 80.9% flow with a delayed scram (TT2).

The ATWS calculation was selected because it would allow an evaluation of the kinetics models under circumstances where the rod effects did not exist. This transient is dominated neutronically by the void and doppler reactivity effects. The scram calculation was selected to study the effects of the rod model since the transient is dominated by the reactivity of the control rods. The last two transients were selected as typical transients on which extensive work has been previously performed (9).

The plant model used is shown in Figure 1. It consists of 35 volumes, 43 junctions and 13 heat conductors. For the one-dimensional kinetics (1-D) and point kinetics obtained by using cross-sections and an infinite time step for the shape function (QPT), the core is divided into 2 inch neutronics mesh intervals. Dynamic slip and implicit numerics were used for all of the calculations. The profile fit subcooled voiding model was used with input bundle coefficients for neutronic feedback. A non-equilibrium volume was used in the upper downcomer region (volume 34) to represent the non-equilibrium effects in the region of the mixture level. For the ATWS and scram calculations, the bypass line was not modeled.

The one-dimensional cross-sections were developed with the SIMULATE-E and SIMTRAN-E computer codes for the point in life of the plant. Three SIMULATE-E cases were run from the end of cycle restart file for each of the different power/flow initial conditions used in this study. They consisted of the initial condition rod pattern (base), all rods out (ARO) and all rods in (ARI). With these cases as input, SIMTRAN-E collapsed the three-dimensional cross-sections to one-dimensional cross-sections and created the RETRAN-02 required polynomial forms for the cross-sections. The Y-functions describing the rod worth were also obtained from SIMTRAN-E.

The equivalent point kinetics parameters for the cross-sections will eventually be calculated directly by SIMTRAN-E. However, this option is not currently available in the released version of the code. Therefore, the equivalent point kinetics parameters were calculated for this paper using other means. The scram curve was obtained by performing a series of steady-state RETRAN calculations using the one-dimensional cross-sections. Each calculation had the rods inserted a different amount. The steady-state eigenvalue determined by each calculation was compared with the eigenvalue obtained with the rods fully out to determine the effect of the rods for each calculated insertion. A scram curve was created from this information. This method is equivalent to the one which is implemented in an experimental version of SIMTRAN-E.

A SIMTRAN-E algorithm for obtaining the equivalent point kinetics parameters for void and doppler reactivity has not been decided upon yet. One possible approach under evaluation was used to perform hand calculations to develop these parameters. The SIMTRAN-E perturbation data was collapsed to develop a doppler coefficient and a void reactivity curve.

The void reactivity curve was based on changes in the core-averaged density. To apply this curve, a control system was included in RETRAN to determine the core-averaged density and to obtain the reactivity effects from the changes in this value. The point kinetics calculations using this approach will be identified as PTC. A second set of point kinetics calculations using this same void reactivity curve in each core volume separately will be identified as PT. The latter approach attempts to bring in some one-dimensional effects (e.g., changes in moderator density in the channel) and is not classical point kinetics. These two approaches will be compared for each transient.

Finally, a second set of cross-sections (and their associated point kinetics parameters) were derived for all of the transients except the ATWS. These were created because of abnormalities in the rod behavior observed in the first set. These abnormalities will be discussed later. The second set was derived in SIMTRAN-E from SIMULATE-E cases for the base and ARI conditions and are identified as 2S. Due to using two cases, this set is somewhat conservative related to rod worth. The effect of the movement of the partially inserted rods is ignored until the scram bank reaches them. This underestimates the amount of reactivity insertion in the early part of the scram. The original set derived from the base, ARO and ARI conditions are identified by 3S.

Experimental versions of SIMTRAN-E and RETRAN have been developed for testing purposes. These versions have a different rod model (which will be described late) and the ability to generate and use region wise (i.e., a different set for each core node) point kinetics parameters. The experimental version can also generate average point kinetics parameters and to generate a scram curve. The results using these experimental code versions will be given in a later section of this paper.

The ATWS transient was initiated by a turbine trip from 100% power and 100% flow conditions. This transient assumed no bypass flow capabilities. Table 1 shows the peak parameters and computational time for each of the four cases, i.e., one-dimensional kinetics (1-D), point kinetics using cross-sections (QPT), point

kinetics using a core-averaged density for reactivity feedback (PTC) and point kinetics using each volume density separately (PT). The running time given is CP seconds on a CDC 6600.

TABLE 1 ATWS

Case*	Peak System Normalized Power	Peak Steam Dome Pressure	6600 CP Sec.
1-D	3.68 @ 0.70	1413.24 @ 22.0	3426.5
QPT	3.81 @ 0.70	1524.76 @ 25.0	2964.5
PTC	3.02 @ 0.96	1461.43 @ 23.25	1929.2
PT	2.50 @ 0.94	1449.70 @ 24.5	1889.7

* 1-D = one-dimensional kinetics, QPT = point kinetics using cross sections, PTC = point kinetics using core-averaged density for reactivity feedback, PT = point kinetics using each volume density separately.

Figure 2 shows the variation of the axial power distribution during the transient. Figures 3 and 4 show respectively, a comparison of the power and steam dome pressure histories for 1-D, QPT, and PTC. Figures 5 and 6 show the comparison of the same parameters for PTC and PT. The plots of the axial power distribution indicate that the assumption of a constant power profile is not a good one. However, the ATWS does not result in as strongly a changing profile as do transients where the control rods are inserted. Ignoring the shape function causes the system to be less damped and adds a time delay in the power history. All three models reach a different equilibrium as shown by the different final power and pressure levels. The comparison of PTC and PT reveals that it is important to use the appropriate form of the cross-section parameters. The point kinetics parameter calculations demonstrate a considerably more damped power behavior than do the calculations using the one-dimensional cross-sections.

A study of the computational times for these transients revealed an unexpected result. For this case the shape function was calculated for approximately 17% of the time steps. The one-dimensional kinetics calculation ran 78% longer than the traditional point kinetics calculation. It was originally anticipated that a major portion of this additional computational time was due to the shape function calculations.

However, the QPT case ran 54% longer than the traditional point kinetics calculation. This demonstrates (along with the other transients) that the evaluation of the cross-sections and inner products in the QX-1 point kinetics requires a substantial amount of time. These cross-section calculations are done at every time step. Updating the cross-sections on this frequency may not be necessary. In the original QX-1 there were time step controllers to determine the frequency of calculation of the shape function, inner products and cross-sections. These controllers were removed when the model was implemented in RETRAN. The intention was to replace them when the interaction of the thermal-hydraulics and neutronics time step controllers was better understood. The large computational time increase in even the QPT case indicates the strong need to speed up the calculational algorithm and to implement the neutronics time step controllers in RETRAN.

The scram transient was initiated by inserting all of the control rods from 100% power and 100% flow conditions. This transient demonstrates pre-dominantly the effects of the control rod model in the one-dimensional cross-sections. The void and doppler reactivity components, although not eliminated, are of a lesser order of importance. Table 2 shows the peak parameters and computational time for each of the four cases using both the 2S and 3S cross-section sets.

Figure 7 shows the variation of the axial power distribution during the transient. Figures 8 and 9 show respectively, a comparison of the power and steam dome pressure histories for 1-D, QPT and PTC using the 2S cross-sections.

The PTC and PT cases are virtually identical as would be expected since the rod worth curve is the dominant reactivity component for this transient. Figure 10 compares the one-dimensional power histories for the 2S and 3S cross-section sets.

The values for the peak power shown in Table 2 for 1-D-3S and QPT-3S indicate the abnormalities in the rod model which sometimes occur when all three SIMULATE-E cases are used. The initial insertion of the scram rods creates a non-physical positive reactivity insertion. The PTC-3S and PT-3S cases do not show this behavior because the scram curve was developed by moving the rod by one foot increments. By the time the rod is inserted one foot, the reactivity insertion is negative. When the two SIMULATE-E cases are used, the initial positive reactivity insertion does not occur. A similar, non-physical abnormality of positive reactivity insertion with rod insertion is seen in TT1 but not in TT2. This situation

points out the importance of evaluating the Y-functions generated by this technique before using the cross-sections. This work shows that it is better to use in this version of the codes the maximum and minimum rod concentration cases actually seen by the specific transient (i.e., for this transient, the base and ARI cases) than all three cases.

TABLE 2 SCRAM

Case	Cross* Section	Peak System Normalized Power	Peak Steam Dome Pressure	6600 CP Sec.
1-D	2S	1.0 @ 0.0	1020.0 @ 0.0	1539.5
QPT	2S	1.0 @ 0.0	1020.0 @ 0.0	1212.3
PTC	2S	1.0 @ 0.0	1020.0 @ 0.0	658.4
PT	2S	1.0 @ 0.0	1020.0 @ 0.0	683.7
1-D	3S	1.46 @ 0.04	1020.0 @ 0.0	1599.5
QPT	3S	1.28 @ 0.04	1020.0 @ 0.0	1275.8
PTC	3S	1.0 @ 0.0	1020.0 @ 0.0	682.2
PT	3S	1.0 @ 0.0	1020.0 @ 0.0	645.0

* 2S = derived from base and ARI conditions, 3S = derived from base, ARO and ARI conditions.

The movement of the control rods in this transient causes considerable changes in the axial power profile. Comparing the 1-D and QPT cases indicated the importance of these power shape changes. Neglecting the power shape changes causes the power to drop much more quickly. The wave effect on the power shown especially in the 1-D case is caused by the different cross-sections in each volume. The slope discontinuities occur at the junction interfaces.

The TT1 transient is a turbine trip with bypass transient initiating at 57.4% power and 100% flow. The anticipatory scram was delayed for this transient. The actual scram was caused by the high flux signal whose setpoint had been lowered. Table 3 shows the peak parameters and computational time for each of the four cases using both the 2S and 3S cross-section sets.

TABLE 3 TT1

Case	Cross Section	Peak System Normalized Power	Peak Steam Dome Pressure	6600* Comp Time
1-D	2S	4.01 @ 0.82	1039.85 @ 3.1	3065.4
QPT	2S	4.05 @ 0.82	1031.41 @ 3.0	3066.4
PTC	2S	2.47 @ 0.96	1038.26 @ 4.0	1864.9
PT	2S	2.36 @ 1.0	1037.77 @ 4.0	1819.4
1-D	3S	10.5 @ 1.02	1069.09 @ 3.2	3561.3
QPT	3S	4.48 @ 0.86	1037.31 @ 3.0	3165.3
PTC	3S	26.7 @ 1.14	1109.91 @ 4.0	1877.5
PT	3S	13.8 @ 1.24	1095.73 @ 4.2	1772.4

* The 1-D 2S case computed 7.8 transient seconds and the QPT 2S case computed 9.25 transient seconds. All of the other cases computed 10.0 transient seconds.

Figure 11 shows the time-dependent behavior of the axial power profile during the transient. Figures 12 and 13 show the comparison of the power and steam dome pressure respectively, for the 1-D, QPT and PTC cases using the 2S cross-sections. Figure 14 compares the one-dimensional power histories for the 2S and 3S cross-section sets.

It can be seen by both the results given in Table 3 and from Figure 14 that the 3S cross-section set over-shoots the power considerably. (The experimentally measured power was 4.65). In the 2S case, the power begins to decrease due to void and doppler reactivity effects. Almost immediately the rods move in to reduce the power rapidly. In the 3S case, the same thing occurs as can be seen by the inflection in the power at about 0.8 seconds. However, due to a non-physical abnormality in the rod Y-functions, positive reactivity is inserted as the rods are inserted causing the much higher non-realistic peak power. This is another case where the base, ARI and ARO combination has caused difficulties with the calculation of the Y-functions. The base and ARI combination behaves as expected.

The 1-D calculation shows that the axial power profile changes during the transient.

This same phenomena was observed in the experiment. The 1-D and QPT calculations both calculate approximately the same peak power; however, the PTC and PT cases both have a much lower value. The latter two cases also have a delayed peak time and an unusual peak shape compared to experimental results.

The TT2 transient is a turbine trip with bypass transient initiating at 61.6% power and 80.9% flow. The anticipatory scram was delayed for this transient. The actual scram was caused by the high flux signal whose setpoint had been lowered. Table 4 shows the peak parameters and computational time for each of the four cases using both the 2S and 3S cross-section sets.

Figure 15 shows the time-dependent behavior of the axial power profile during the transient. Figures 16 and 17 show respectively, the comparison of the power and steam dome pressure for the 1-D, QPT and PTC cases when the 2S cross-sections are used. Figure 18 compares the one-dimensional power histories for the 2S and 3S cross-section sets.

For TT2, it can be seen that the 2S and 3S cross-sections give similar results. For this transient and its initial power distribution, the control rod model abnormality is not observed. This does not however, affect the recommendation, that for the present rod model in RETRAN, it is better to use the 2S type set of cross-sections, even though it is somewhat conservative when the rods move.

TABLE 4 TT2

Case	Cross Section	Peak System Normalized Power	Peak Steam Dome Pressure	6600 Comp Time
1-D	2S	2.72 @ 0.76	1052.84 @ 3.9	3546.4
QPT	2S	2.69 @ 0.76	1039.70 @ 2.9	3155.1
PTC	2S	1.84 @ 0.96	1056.33 @ 3.9	1829.9
PT	2S	1.88 @ 0.92	1056.03 @ 3.9	1857.4
1-D	3S	2.70 @ 0.76	1046.04 @ 3.0	3597.7
QPT	3S	2.68 @ 0.76	1037.11 @ 2.9	3192.8
PTC	3S	1.84 @ 0.96	1052.98 @ 3.9	1876.9
PT	3S	1.87 @ 0.92	1052.47 @ 3.9	1768.3

In all cases, the peak power is underestimated since the experimental value was 4.52. This may be caused by performing a Haling calculation instead of a detailed SIMULATE burn calculation to the test point. Matching the experiment was not the main objective of this paper, so the detailed calculation was not performed at this time. It will be in the future. As was the case in TT1, the PTC and PT cases calculated a lower peak value than the cross-section cases, 1-D and QPT. Again, as seen in TT1, the PTC and PT show a delayed peak time and an unusual peak shape compared to the experimental results.

CONTROL ROD MODEL

The primary task of the control rod model is to provide a mechanism which modifies the cross-sections when the simulated rod bank is inserted or withdrawn. This is accomplished through the control fraction or F-function which alters the regional group constants depending upon the amount of control rods present.

In its original formulation (10) the F-function was restricted to a range between 0.0 and 1.0. The function is defined from the following equation:

$$\text{Sigma}(I,X) = F(I,X)\ \text{Sigma C}(I,X) + (1.0 - F(I,X))\ \text{Sigma UC}(I,X). \qquad (1)$$

In this equation, the terms are defined as:

Sigma (I,X) = Cross-Section for Region I, Reaction Type X
Sigma C(I,X) = Cross-Section for Region I, Reaction Type X Maximum Rods
Sigma UC(I,X) = Cross-Section for Region I, Reaction Type X Minimum Rods
F(I,X) = Control Fraction for Region I, Reaction Type X

From equation (1), when F = 1.0 the Region is completely controlled or rodded and when F = 0.0 the Region is uncontrolled. Another way of limiting F between 0.0 and 1.0 is to state:

$$\text{Sigma C}(I,X) \leq \text{Sigma}(I,X) \leq \text{Sigma UC}(I,X), \text{ or;}$$
$$\text{Sigma UC}(I,X) \leq \text{Sigma}(I,X) \leq \text{Sigma C}(I,X)$$

That is, the cross-section must always lie between the uncontrolled and the controlled states.

In some cases in SIMTRAN-E this is not always true. The radial collapsing procedure (which includes the effect of the radial flux shape) can generate cross-sections for which the above assumption is violated. The result is an F-function that may be negative, non-bounded (i.e., F > 1.0) or oscillatory in its axial shape. The result may be rod worth curves that are non-physical and lead to the abnormalities demonstrated above.

A detailed explanation of this behavior is beyond the scope of the present work, but the basic deficiency is that the F-function includes both control rod insertion and flux redistribution effects. Additional studies are underway which investigate separating the mechanical effect from the distributional effect. Preliminary results from this work indicate:

1. The control rod model in RETRAN needs modification. An approach such as the F-functions contain rod effects but not flux redistribution effects and stay between 0.0 and 1.0 is being evaluated. The results using this model for the above four transients is presented below.

2. The cross-sections are probably better evaluated from minimum and maximum rod conditions rather than from all rods out and all rods in conditions.

The Y-function which are fed to RETRAN are generated from the F-function and are used to recreate them during the transient calculations.

A new control rod model for RETRAN has been developed and implemented into an experimental version of SIMTRAN-E and RETRAN. In this model the cross sections are evaluated around their initial values and consider only minimum and maximum rod conditions. The cross sections are:

$$\text{Sigma}\ (Z,X) = G(Z)\ \text{Sigma}\ C(Z,X) + \text{Sigma}\ B(Z,X)\ (1.0-G(Z))$$

where

Sigma B(Z,X) = Base case cross section for reaction type X at Z.

Sigma C(Z,X) = maximum rodded cross section for reaction type X at Z.

The new G-functions represent the rod effects only and only have values between 0 and 1.

$$G(Z) = \frac{CFR(Z)-CF(Z)}{CFC(Z)-CF(Z)}$$

where

CFC(Z) = maximum rodded control fraction
CFR(Z) = rod control fraction during scram
CFR(Z) = base case rod control fraction

CF(Z) is derived from the CT(X,Y,Z) control variable in SIMULATE-E. This formalization eliminates the difficulties seen above with the 3S method. Also it does not neglect the effect of the partially inserted rods as the 2S approach did.

This experimental version of SIMTRAN-E calculates two sets of point kinetics parameters. The first is a set of region wise parameters i.e., different void and doppler parameters for each core node.

This approach brings in some one-dimensional effects (i.e., one-dimensional cross section feedback effects). RETRAN was modified to accept these parameters. The calculations using this approach will be identified as PTR. The second set calculates core average point kinetics parameters. The calculations using this approach will be identified as PTA. This version of SIMTRAN-E calculates the rod scram curve for point kinetics calculations.

For each of the four transients (ATWS, SCRAM, TT1, TT2), four calculational methods were used with the experimental versions of SIMTRAN-E and RETRAN. There are one-dimensional kinetics (1-D), point kinetics using cross sections (QPT), region wise point kinetics (PTR) and core average point kinetics (PTA). It should be noted that the latter did not use a control system to get an average core density as done in PTC but instead used the calculated nodal value as is normally done. The results for these calculations are summarized in Table 5.

Figures 19 and 20 show respectively, a comparison of the power and steam dome pressure histories for ATWS transient using all four methods. All except PTA have very similar power behaviors with the point kinetics calculations being less damped than the 1-D calculation. The PTA considerably underestimates the power and therefore the pressure history. The less damped power histories of QPT and PTR cause substantial over-estimate of their pressure histories.

Figures 21 and 22 show the calculated results of power and steam dome pressure

respectively for the SCRAM transient. The new control rod model behaves as expected for this case. It does not have the non-physical effects seen with the 3S cross sections nor is it overly conservative as was seen with the 2S cross sections. The QPT over-estimates the rod worth because the initial flux distribution is used throughout the transient as a weighting factor.

Since the initial flux is higher in the regions where the rods are moving in than it should be, the weighting factor is too high and, therefore, the rod worth is too high. This causes the power to drop too rapidly as seen in Figure 21. The point kinetics calculations PTR and PTA do not have this problem. Although the flux shape is kept constant during the transient, as it was for QPT, the rod worth is not calculated during the transient. In these two cases the scram curve was calculated by SIMTRAN-E a priori. SIMTRAN-E calculates the rod worths by performing a series of steady state calculations with the rod bank at different positions. In this case, the flux used for weighting purposes is the steady state flux for each rod position. In rodded positions this flux is less than the transient initial flux so the rod worth is less and as seen in Figure 21 the power decreases less rapidly than QPT. PTR's calculated power drops more rapidly than PTA's due to the different void and doppler reactivity feedback approaches.

The one-dimensional calculation (1-D) shows a faster power decrease and, therefore, a larger rod worth than the PTR calculation. This is because the former takes the transient behavior of the flux into account when calculating the rod worth. In the region where the rods have been inserted, the flux shape due to prompt neutrons is similar to the steady state flux used in calculating the scram curve for PTR and PTA. However, the flux shape due to delayed neutrons is closer to the initial shape in the early part of the transient. Therefore, the transient flux in the regions where the rod has moved in is larger than the steady state flux. Using the transient flux as a weighting factor gives a higher rod worth and the power drops more rapidly as seen in Figure 21.

Figure 23 compares the scram curves calculated by the three-dimensional calculation in SIMULATE-E and the one-dimensional calculation in SIMTRAN-E for TT1. Figure 24 shows the same for TT2. The fact that the curves compare well demonstrate that the rod model using one-dimensional cross sections compares well with the three-dimensional calculation.

Figures 25 and 26 show the calculated results of the power and steam dome pressure

histories, respectively, for TT1. Again, it can be seen that the rod model behaves as physically expected. The second power peak shown in Figure 25 at 2.2 seconds is no longer a pronounced peak as it was with the 2S cross sections. This is because the rod worth is no longer conservative due to the partial inserted rods. The PTA considerably underestimates the power.

TABLE 5

	Peak System Power	Peak Dome Pressure (PSIA)	CP Time (Sec)
ATWS			
1-D	3.43 @ 0.70	1413.30 @ 23.0	3287.9
QPT	3.61 @ 0.90	1518.46 @ 25.25	2975.3
Point (region)	4.13 @ 0.68	1525.37 @ 24.75	1851.9
Point (core)	1.92 @ 0.64	1315.86 @ 30.0	2685.5
SCRAM			
1-D	1.0 @ 0.0	1020.0 @ 0.0	1410.4
QPT	1.0 @ 0.0	1020.0 @ 0.0	1196.9
Point (region)	1.0 @ 0.0	1020.0 @ 0.0	657.9
Point (core)	1.0 @ 0.0	1020.0 @ 0.0	630.4
TT1			
1-D	4.45 @ 0.80	1030.62 @ 3.0	3339.5
QPT	4.47 @ 0.82	1027.95 @ 2.0	3027.4
Point (region)	3.80 @ 0.84	1029.61 @ 3.0	1755.8
Point (core)	1.79 @ 0.94	1026.65 @ 3.0	1816.0
TT2			
1-D	2.75 @ 0.74	1034.59 @ 2.9	3339.0
QPT	2.68 @ 0.74	1031.33 @ 2.9	3057.5
Point (region)	2.39 @ 0.74	1035.15 @ 2.9	1772.81
Point (core	1.55 @ 0.64	1030.91 @ 2.9	1859.9

Figures 27 and 28 show the calculated values of the power and steam dome histories, respectively, for TT2. The same comments made above for TT1 apply to TT2.

The calculations using the new control rod model show that it is a considerable improvement over the old one. They also show that the region wise point kinetics calculation (PTR) does a much better job than the core average calculation (PTA).

CONCLUSION FROM THE BWR STUDY

1. The control rod model as presently formulated has difficulties in certain cases. With the present model it appears better to run the minimum and maximum rod concentration cases for the transient rather than the base, ARI and ARO cases. When this is done with the present rod model, the movement of the partially inserted rods is ignored until the scram bank reaches them. This underestimates the reactivity insertion in the early part of the scram.

2. The equivalent point kinetics parameters as hand calculated do not adequately represent the transient studied. There appear to be two contributing difficulties.

   First, the inherent neglect of any axial shape function changes. Second, calculating a single void reactivity curve for a core average density appears to smear the phenomena out too much. The latter effects may be extremely important even in cases where the shape function does not change much. A better approach may be to develop a void reactivity curve for each axial node. The perturbations used to develop each curve will be performed over the expected changes at that axial level during the transient. This appraoch is being explored for inclusion in SIMTRAN-E and RETRAN.

3. The present scheme of calculating the cross-sections and inner products at every time step is extremely costly. At the same time having the user determine how often the shape function should be calculated is inefficient. The original QX-1 computer code, which was the developmental base for the factorization method, had time step controllers which determined

how often the shape function, inner products and cross-sections needed to be calculated. These time step controllers or something similar should be implemented in RETRAN to speed up the computational time.

4. The proposed control rod model implemented in the experimental versions of SIMTRAN-E and RETRAN does a very good job on the transients performed in this study. It appears to be a considerable improvement over the presently implemented model in the released versions of the code.

5. The region wise point kinetics calculations (PTR) are substantially better than the core average point kinetics calculations (PTA). There is no additional effort in using the PTR method in either computational time or man hours; therefore, it is highly recommended that the PTR approach be used when point kinetics calculations are desired.

6. In certain transients the axial power distribution changes considerably. To represent this accurately, one-dimensional kinetics calculations must be performed. In other transients the axial power distribution does not change very much during the period of interest and one-dimensional kinetics is not needed. The use of one-dimensional kinetics should be determined by the transient being studied and the important results required in that study.

7. The SIMULATE-E, SIMTRAN-E, RETRAN-02 approach is a very workable means for performing transient analysis. It is important to calculate the cross-sections at the proper conditions to be used in RETRAN. This requires the SIMULATE-E cases to be run at the actual initial conditions of the transient and using the history to the point in life of the plant. This procedure is required to assure that the cross-sections properly reflect their dependencies on density, temperature, etc. These dependencies are important since they determine the transient reactivity effects.

PWR ANALYSIS

The second set of calculations were performed on a Westinghouse four-loop plant using RASP methodology. RASP codes, CELL-2 (11), PDQ7-E (12), NORGE-P (13), NODEP-2, SIMULATE-E, SIMTRAN-E, NODETRAN, and RETRAN were utilized in an attempt to compare the kinetic parameters generated by NODEP-2 - NODETRAN and SIMULATE-E - SIMTRAN-E paths for RETRAN.

In this preliminary study, a simplified core of one fuel type, of 2.248% enrichment, at the beginning of life, cycle one was assumed. Results from CELL-2 calculations performed at three moderator temperatures; 525 degrees F, 560 degrees F and 650 degrees F, with no depletion were used in PDQ7-E color set calculations to generate assembly parameters for the nodal codes. NORGE-P was then used to process these parameters for NODEP-2 and SIMULATE-E respectively.

Two cases, all rods out (ARO) and all rods in (ARI), for both NODEP-2 and SIMULATE-E were run under the same initial conditions as those later used in RETRAN analyses. The boron concentration was set at 1235.0 ppm. The FLARE type calculations were selected in the SIMULATE-E calculation in order to be the most comparable with NODEP-2.

The steady state relative power distribution by assembly and the core average axial power are compared in Figure 29. The eigenvalues and relative power distribution by assembly under both ARO and ARI conditions show good agreement. The core average axial power, obtained from SIMULATE-E is slightly more bottom peaked than that of NODEP-2. The rod worth of SIMULATE-E and NODEP-2 are 0.0693 and 0.0684 respectively. These eigenvalues and those calculated by RETRAN using cross sections generated by the NODEP-2, NODETRAN and SIMULATE-E, SIMTRAN-E paths are compared in Table 6 later.

The processing of delay neutron data from CELL-2 was automated by using the NTPREP code which then feeds into NODETRAN along with the 3-D cross-sections obtained from NODEP-2. NODETRAN then uses both data sets to generate one-dimensional parameters for RETRAN. For this study, a test version of NODETRAN which produces the core average point kinetics parameters from the cross-sections, moderator density and doppler reactivities were used. However, the delay neutron data were hand calculated and fed into SIMTRAN-E. It should be noted that the experimental version of SIMTRAN-E and RETRAN as described in the BWR analyses are used in the SIMULATE-E, SIMTRAN-E, RETRAN path whereas RETRAN-02 MOD003 is used

in the NODEP-2, NODETRAN, RETRAN path.

The scram curves shown in Figure 30 were obtained by performing a series of steady state RETRAN calculations using the one-dimensional cross sections for both paths. Each calculation had the rods inserted a different amount. Table 6 shows the eigenvalues calculated by (1) NODEP-2, (2) SIMULATE-E, (3) RETRAN using 1-D parameters from NODEP-2 - NODETRAN, (RETRAN-N) and (4) RETRAN using 1-D parameters from SIMULATE-E - SIMTRAN (RETRAN-S). All eigenvalues are in excellent agreement except for the RETRAN-N case, especially under the ARI condition. The large eigenvalue deviation between NODEP-2 and RETRAN-N is now being investigated.

TABLE 6 COMPARISON OF EIGENVALUES

	ARO	ARI	$\Delta\rho$
NODEP-2	1.0389	0.9700	0.0684
RETRAN-N	1.0428	0.9961	0.0450
SIMULATE-E	1.0425	0.9723	0.0693
RETRAN-S	1.0425	0.9722	0.0693

Three transients were selected in RETRAN analyses. They are:

1. Complete loss of flow without scram (ATWS(LOF))

2. Scram

3. Complete loss of flow (LOF).

The plant model used is shown in Figure 31. It consists of 65 volumes, 91 junctions, 21 heat conductors including 12 core sections each divided into 2 inch neutronics mesh intervals. Dynamic slip and implicit numerics were used. PWR guidelines for RASP were followed to set up plant initial conditions at 102% power and rated flow with 4 degrees F core inlet temperature deadband drift and -30 psi pressurizer pressure uncertainty assumed.

All transients were initiated at 1.0 seconds. For each of the three transients, one-dimensional kinetics (1-D) and point-kinetics using cross-sections (QPT) were used for both RETRAN-N and RETRAN-S paths. In the QPT calculations for all three

transients, the shape function was set to change at each actual time step from the onset of the transient for the first four seconds of transient time. For the next five seconds the shape function was calculated every 10 time steps. All transient calculations terminated at 10 seconds.

As for the point kinetics calculations, core average point kinetics parameters generated by NODETRAN were used in the RETRAN-N path. For RETRAN-S path, two cases, one using region wise point kinetics parameters (PTR) and the other using the core average point kinetics parameters (PTA) generated by the experimental version of SIMTRAN-E were used. It should be noted that RETRAN-02 MOD003 was used in RETRAN-N path and the experimental version of RETRAN with the proposed rod model was used in RETRAN-S path for all calculations.

The sequence of events of ATWS (LOF) transient is: all RCP pumps tripped 1.0 seconds, feedwater isolation valves and turbine stop valves tripped to close at 2.3 seconds and pressurizer PORV/SRV tripped open at 5 seconds, 8 seconds and 9 seconds. Results are presented in Figures 32, 33, and 34.

Without a scram in this transient, the power shape remained nearly the same during the first few seconds and is reflected in the extreme closeness of the 1D, point-kinetics with cross-section, and region wise power kinetics core average temperature results. However, the shape function did change as transient progresses causing the QPT and region wise point kinetics (PTR) to overestimate whereas both core average point kinetics results in RETRAN-N and RETRAN-S paths show damped effect.

The scram was initiated at 1.0 seconds in the second transient, no other action occurred. Results are presented in Figures 35, 36, and 37. Since all RCPs remained operating, no core average temperature peak was observed. Similar to the BWR scram results, keeping the shape function constant causing the rod worth to be too high for QPT, whereas in PTC, PTR and PTA cases, the rod worth is too low due to the fact that scram curve was obtained by a series of steady state calculations with rod bank at various locations.

All four reactor coolant pumps started coasting down at 1.0 seconds in the LOF transient. The reactor scrammed at 2.2 seconds, feedwater isolation valve and turbine stop valves tripped to close at 2.0 seconds. Axial power profile change, system normalized power and core average temperature during the transient are shown in Figures 38, 39, and 40. As observed in BWR cases, the point kinetics

power history shows a time delay. All three models reach a different equilibrium in power history. Similar to scram results, rod worth differences cause point kinetics models to overpredict whereas QPT model to underestimate the results. In all cases, the differences in core average temperature are within 3 degrees F.

System normalized power, peak core average temperature and CDC 6600 computing time for all PWR cases are summarized in Table 7. For RETRAN-N path, the average computing time increase over point kinetics calculations is ~65% for 1-D model and ~35% for QPT model. For RETRAN-S path, the region wise and core average point kinetics models show nearly the same computing time. The improved neutronics calculation schemes in the experimental RETRAN also reduces the computing time penalty for 1-D and QPT to ~40% and ~25% respectively.

TABLE 7A, PWR RESULTS - RETRAN-N PATH

	Peak System Power	Peak Core TAVG F	CP Time (Sec.)
ATWS			
1-D	1.105 @ 7.6	597.7 @ 10.0	779.2
QPT	1.102 @ 8.4	598.0 @ 10.0	674.4
PT	1.000 @ 1.1	593.7 @ 10.0	468.8
SCRAM			
1-D	1.003 @ 1.0	568.9 @ 1.0	740.8
QPT	1.000 @ 1.0	568.9 @ 1.0	606.2
PT	1.000 @ 1.0	569.2 @ 1.0	460.6
LOF			
1-D	1.019 @ 2.4	573.7 @ 3.2	778.8
QPT	1.016 @ 2.1	573.3 @ 3.0	614.9
PT	1.000 @ 1.1	573.8 @ 3.3	460.6

CONCLUSION FROM THE PWR STUDY

Even though a highly simplified core condition was assumed in this preliminary study, it has proved to be adequate in demonstrating RASP methodology from basic lattice physics analysis to system transient analysis. This study also provides a qualitative means to compare the two parallel methods, i.e., NODEP-2 - NODETRAN - RETRAN (RETRAN-N) and SIMULATE-E - SIMTRAN - RETRAN (RETRAN-S) paths. The following are observed:

1. The excellent agreement between NODEP-2 and SIMULATE-E results indicates that RASP methodology has successfully processed lattice data (CELL-2) through assembly calculation (PDQ7-E) and through the linkage code NORGE-P to the nodal codes.

TABLE 7B PWR RESULTS - RETRAN-S PATH

	Peak Core Power	Peak Core TAVG F	CP Time (Sec.)
ATWS			
1-D	1.064 @ 7.4	597.74 @ 10.0	672.2
QPT	1.197 @ 10.0	599.89 @ 10.0	608.0
Point (region)	1.187 @ 10.0	599.65 @ 10.0	499.1
Point (core)	1.004 @ 2.2	594.19 @ 10.0	487.0
SCRAM			
1-D	1.002 @ 10.0	569.04 @ 9.3	659.6
QPT	1.000 @ 1.0	569.14 @ 1.0	588.5
Point (region)	1.000 @ 1.0	569.07 @ 1.0	469.1
Point (core)	1.000 @ 1.0	569.07 @ 9.0	469.2
LOF			
1-D	1.014 @ 2.1	573.94 @ 3.2	673.6
QPT	1.013 @ 2.1	573.44 @ 3.0	592.0
Point (region)	1.012 @ 2.2	574.10 @ 3.3	480.6
Point (core)	1.004 @ 2.2	574.22 @ 3.4	479.4

2. Because of power profile change during transients studied here, the 1-D model would produce more accurate results. The system normalized power history during LOF and scram transients are overestimated by using point-kinetics models. The resulting core average temperature is also lower for the 1-D case. In loss-of-flow analysis, when DNBR is a limiting factor, using 1-D model may gain additional margin.

3. Large discrepancy between NODEP-2 eigenvalue and that obtained by RETRAN-N suggests a likely error in the test version of NODETRAN. Efforts are now underway to investigate this difference.

4. For the three transients studied, the average increase on 6600 CP time over point kinetics calculation is 40% to 65% for 1-D model and 25% to 35% for point kinetics with cross-sections model. The neutronics calculation scheme used in RETRAN-S results in more than 10% computing time saving for 1-D and QPT over the current scheme used in RETRAN-N. As in the BWR results, the use of the region wise point kinetics calculations (PTR) is highly recommended in PWR analysis.

5. In general, RETRAN results obtained from these two methods show the same trend indicating that these two methods are very comparable. Because of the higher rod worth in the RETRAN-S method, power profile shows a larger change during transient with scram leading to larger difference between 1-D and point kinetics results.

REFERENCES

1. N.H. Larsen, Core Design and Operating Data for Cycles 1 and 2 of Peach Bottom 2, EPRI NP-563, June 1978.

2. L.A. Carmichael and R.O. Niemi, Transient and Stability Tests at Peach Bottom Atomic Power Station Unit 2 at End of Cycle 2, EPRI NP-564, June 1978.

3. D.A. Memeley, K.O. Ott and E.S. Wiener, Space Time Kinetics - The QX-1 Code, ANL-7310, 1967.

4. J.H. McFadden et al, RETRAN-02 - A Program for Transient Thermal-Hydraulic Analysis of Complex Fluid Flow Systems, EPRI NP-1850, May 1981.

5. D.M. VerPlanck et al, SIMULATE-E: A Nodal Core Analysis Program for Light Water Reactors, EPRI NP-2792-CCM, March 1983.

6. B.M. Rothleder et al, Advanced Recycle Methodology Program System Documentation, Part II, Chapter 14, EPRI Draft, March 1983.

7. G.C. Gose et al, SIMTRAN-E - A SIMULATE-E to RETRAN-02 Datalink, EPRI Draft, October 1983.

8. R.D. Mosteller et al, NODETRAN: A PWR Datalink from EPRI NODE-P and Other ARMP Codes to RETRAN, EPRI Draft, December 1982.

9. K. Hornyik and J.A. Naser, RETRAN Analysis of the Turbine Trip Tests at Peach Bottom Atomic Power Station Unit 2 at the End of Cycle 2, EPRI NP-1076-SR, April 1979.

10. H.S. Cheng, Scram Bank and Rod Drop Simulations, BNL-20059, 1976.

11. W.R. Cobb et al, Advanced Recycle Methodology Program System Documentation, Part II, Chapter 5, EPRI Report, February 1983.

12. G.R. Poetschat, Advanced Recycle Methodology Program System Documentation, Part II, Chapter II, Chapter 9A, EPRI Report, January 1984.

13. W.R. Cobb et al, NORGE-P Code Description, EPRI Draft, April 1983.

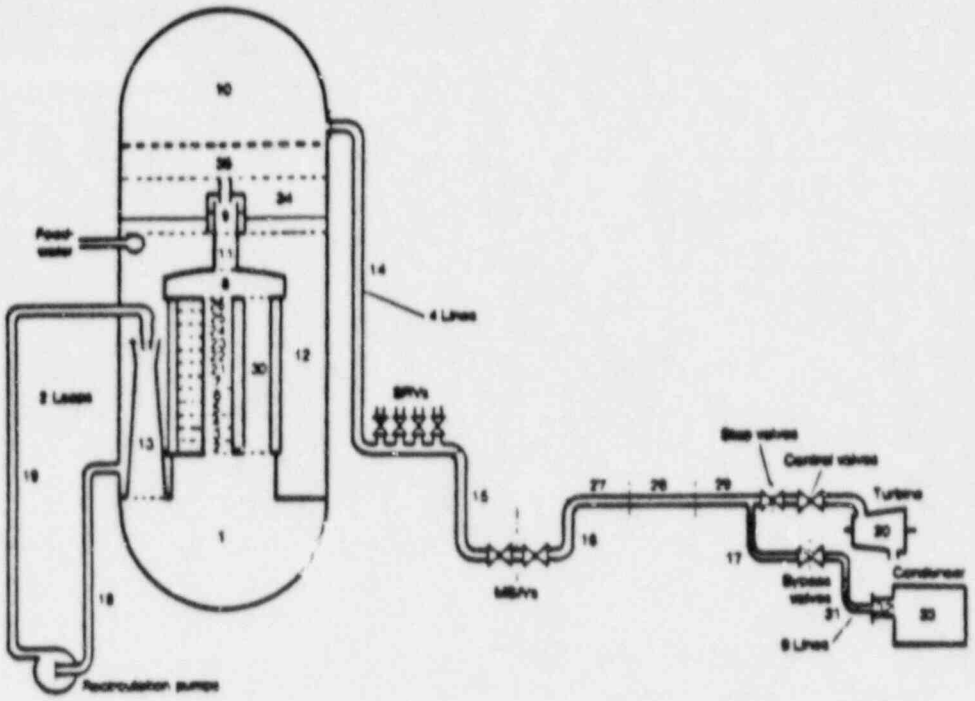

Figure 1 Schematic of Plant Model

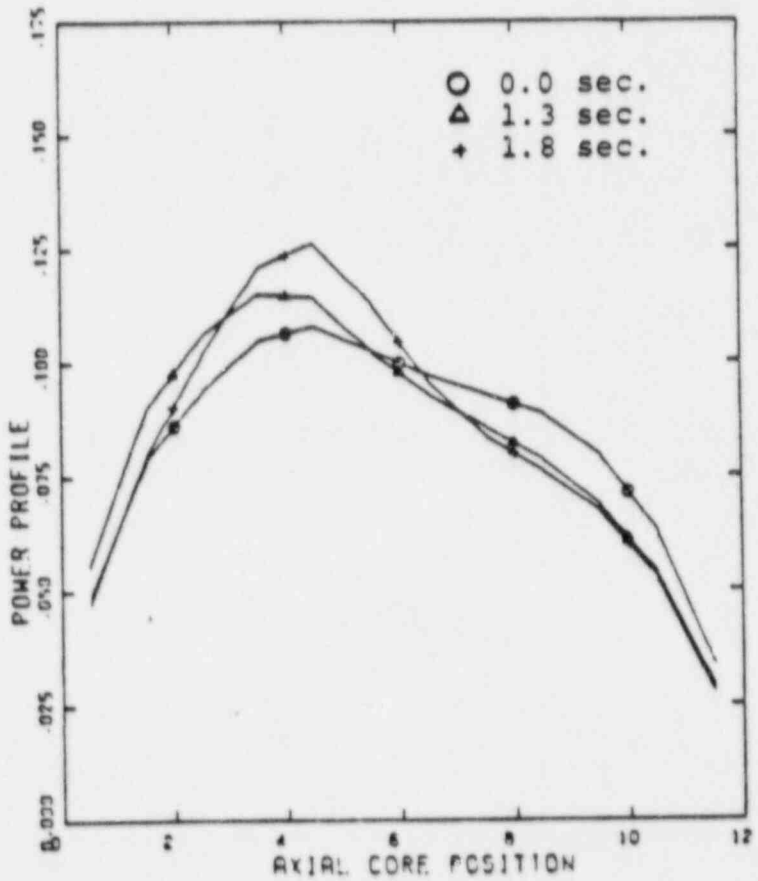

Figure 2 Axial Power Profiles During ATWS

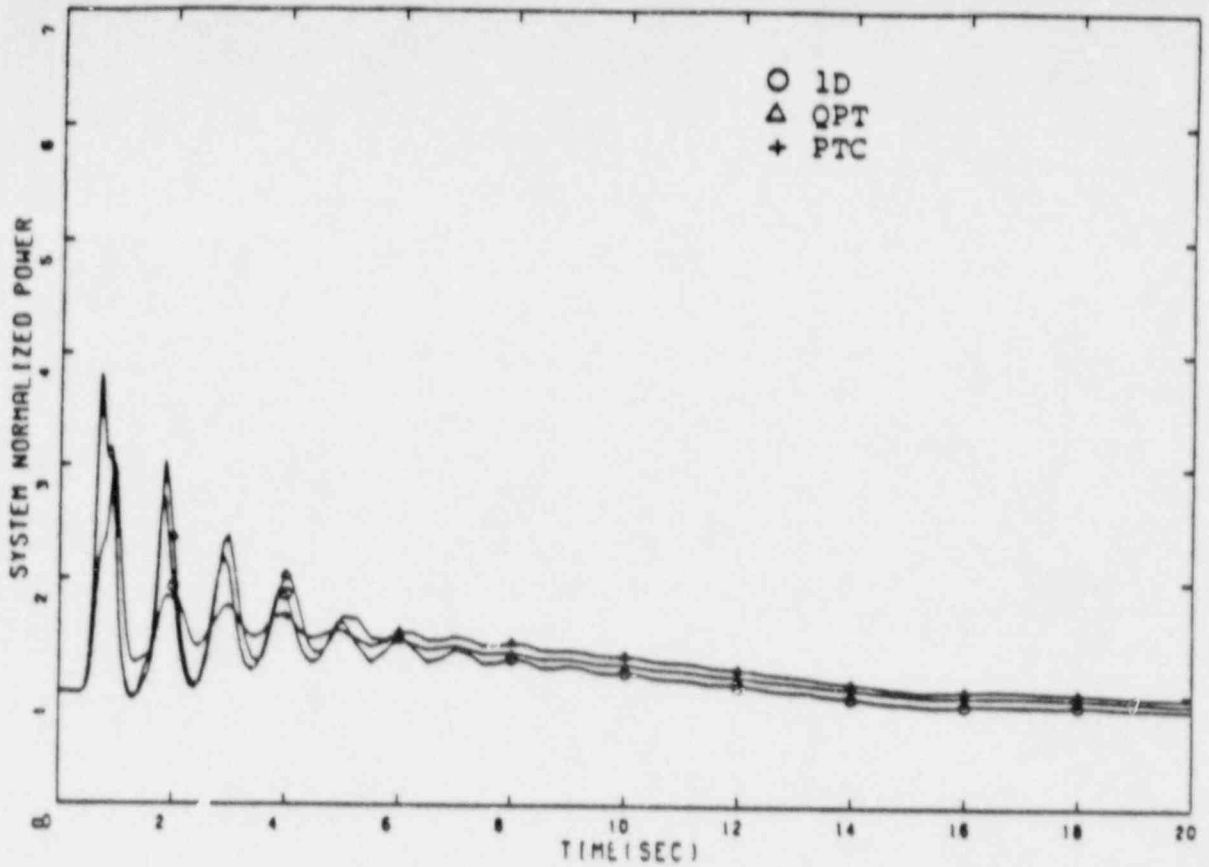

Figure 3 Comparison of System Normalized Power During ATWS

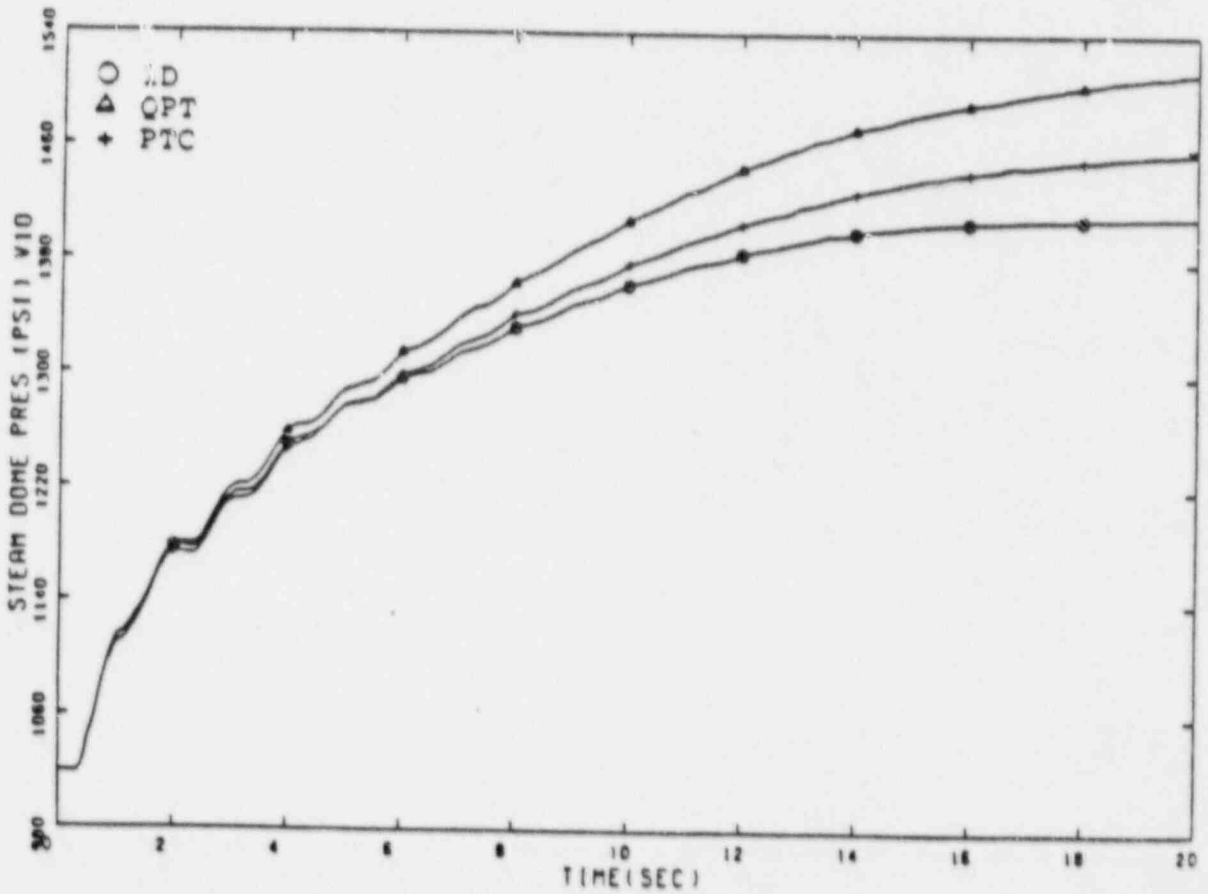

Figure 4 Comparison of Steam Dome Pressure During ATWS

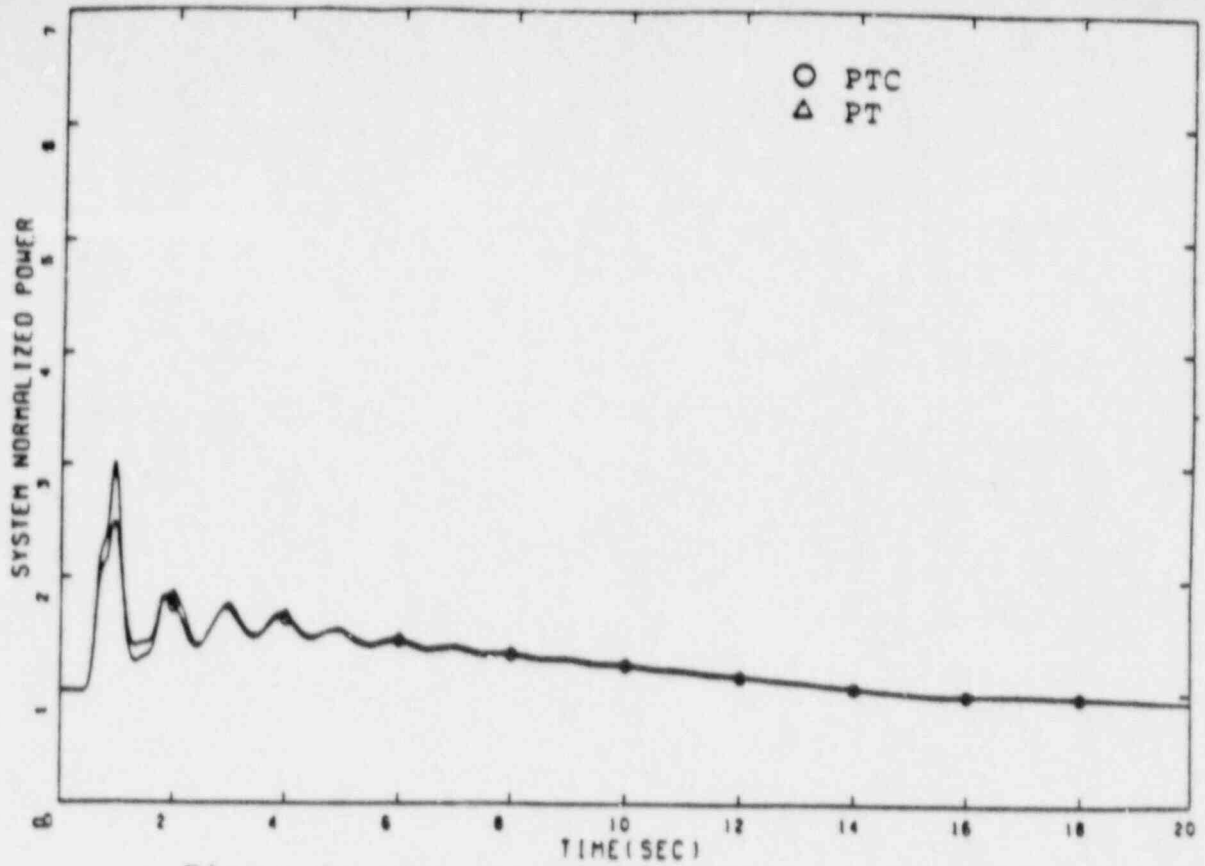

Figure 5: Comparison of System Normalized Power Using Core Averaged and Volume Averaged Quantities

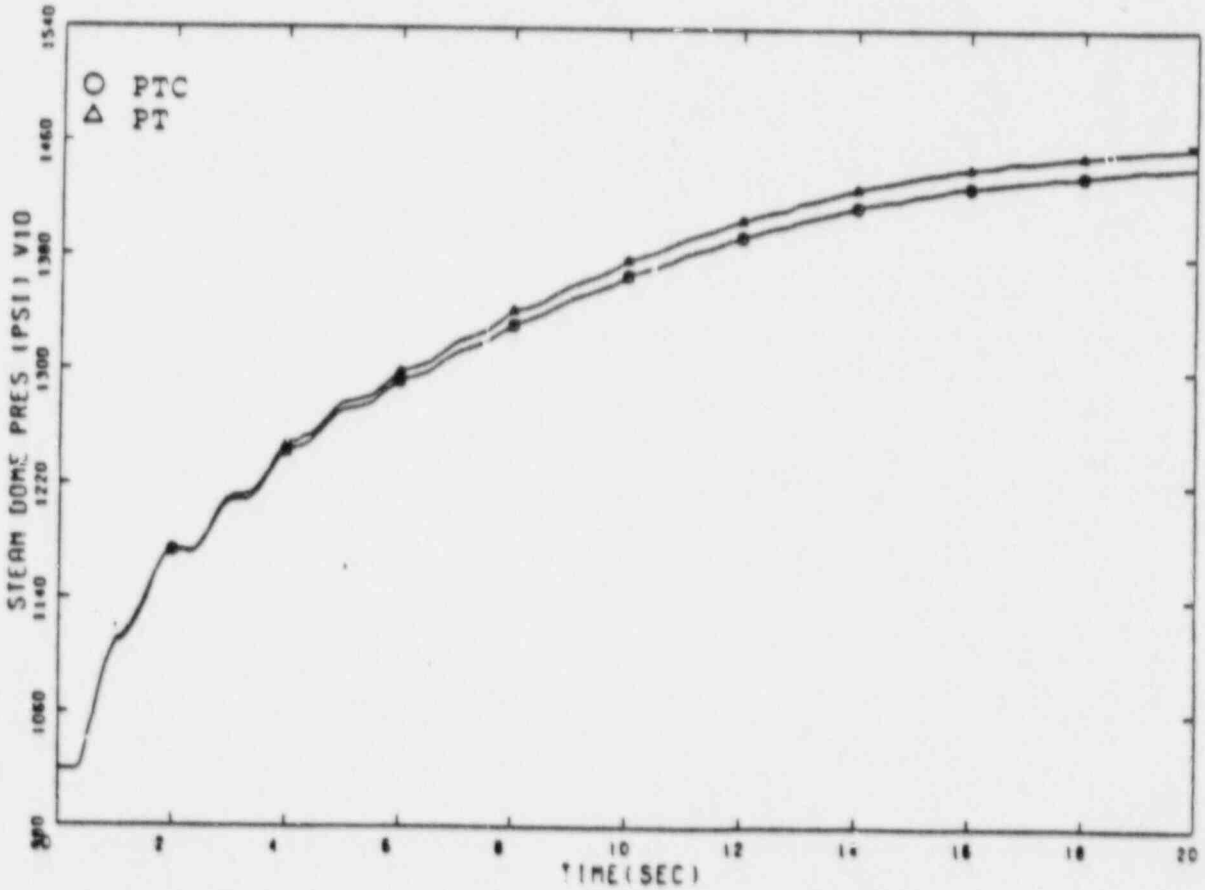

Figure 6 Comparison of Steam Dome Pressure Using Core Averaged and Volume Averaged Quantities

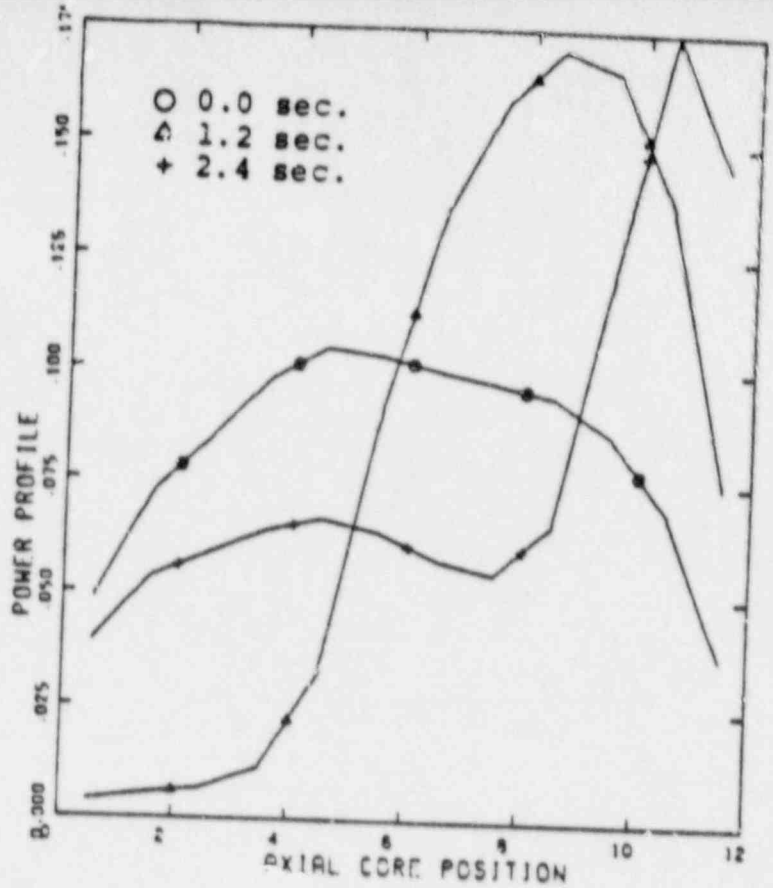

Figure 7 Axial Power Profiles During Scram Transient

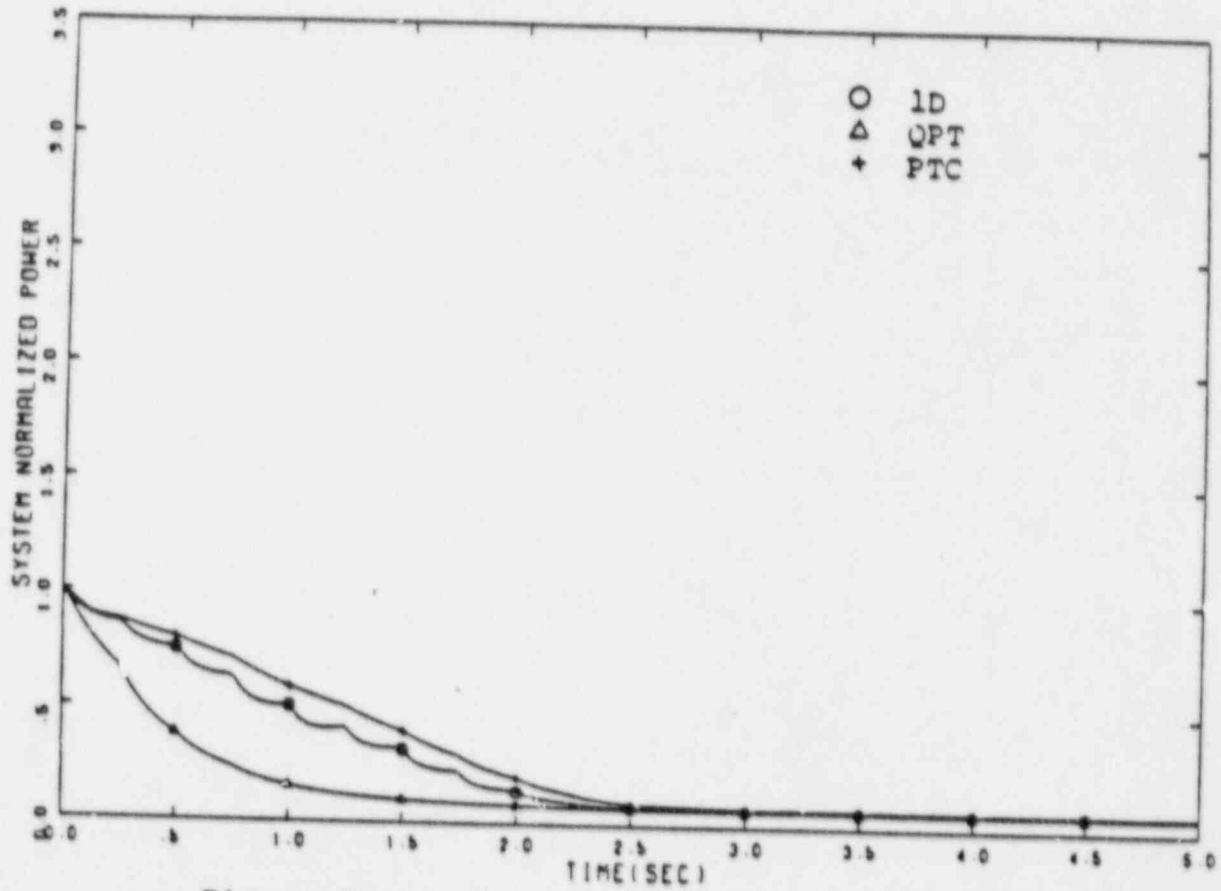

Figure 8 Comparison of System Normalized Power During Scram Transient

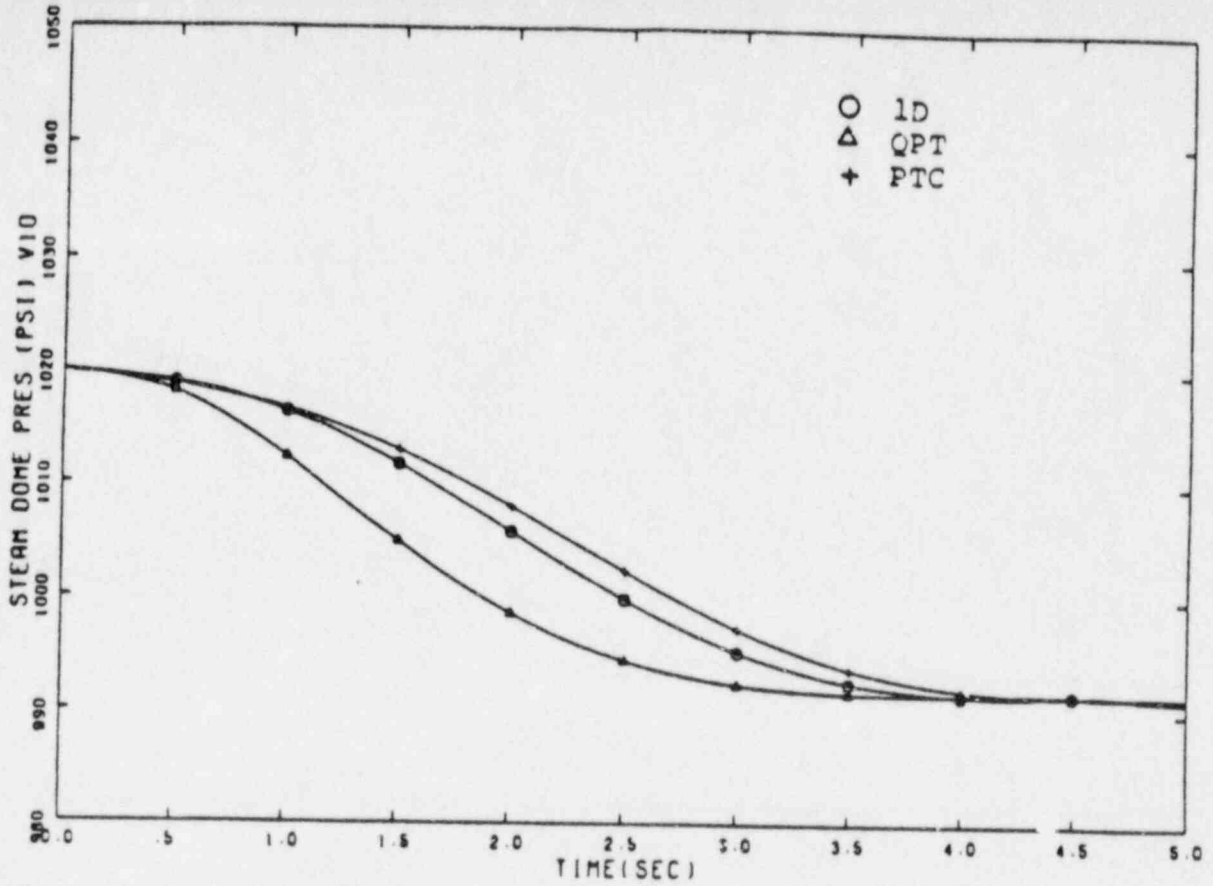

Figure 9 Comparison of Steam Dome Pressure During Scram Transient

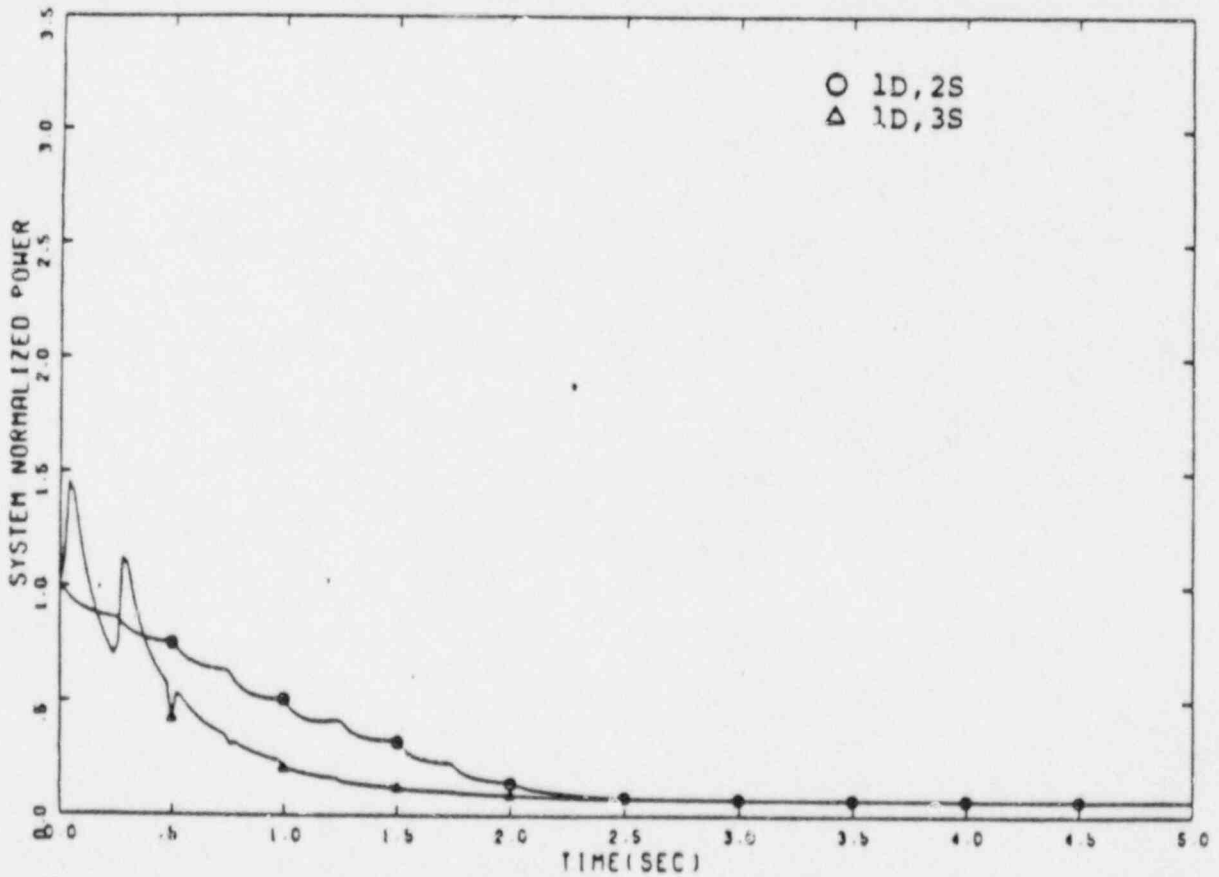

Figure 10 Comparison of Power Calculated by One-Dimensional Kinetics Using the 2S and 3S Cross-Section Sets for the Scram Transient

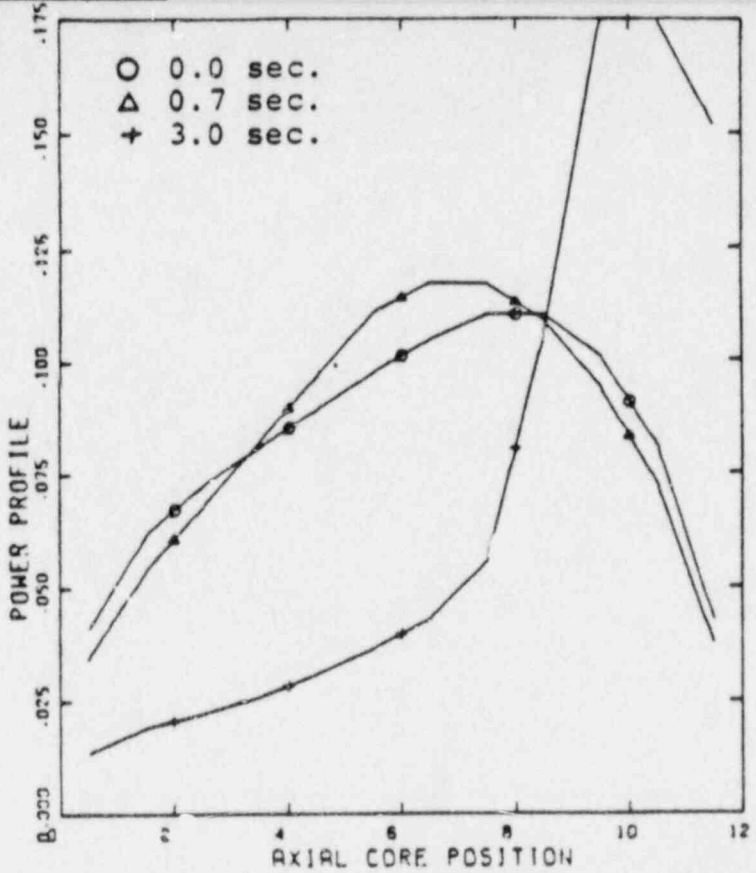

Figure 11 Axial Power Profiles During TT1

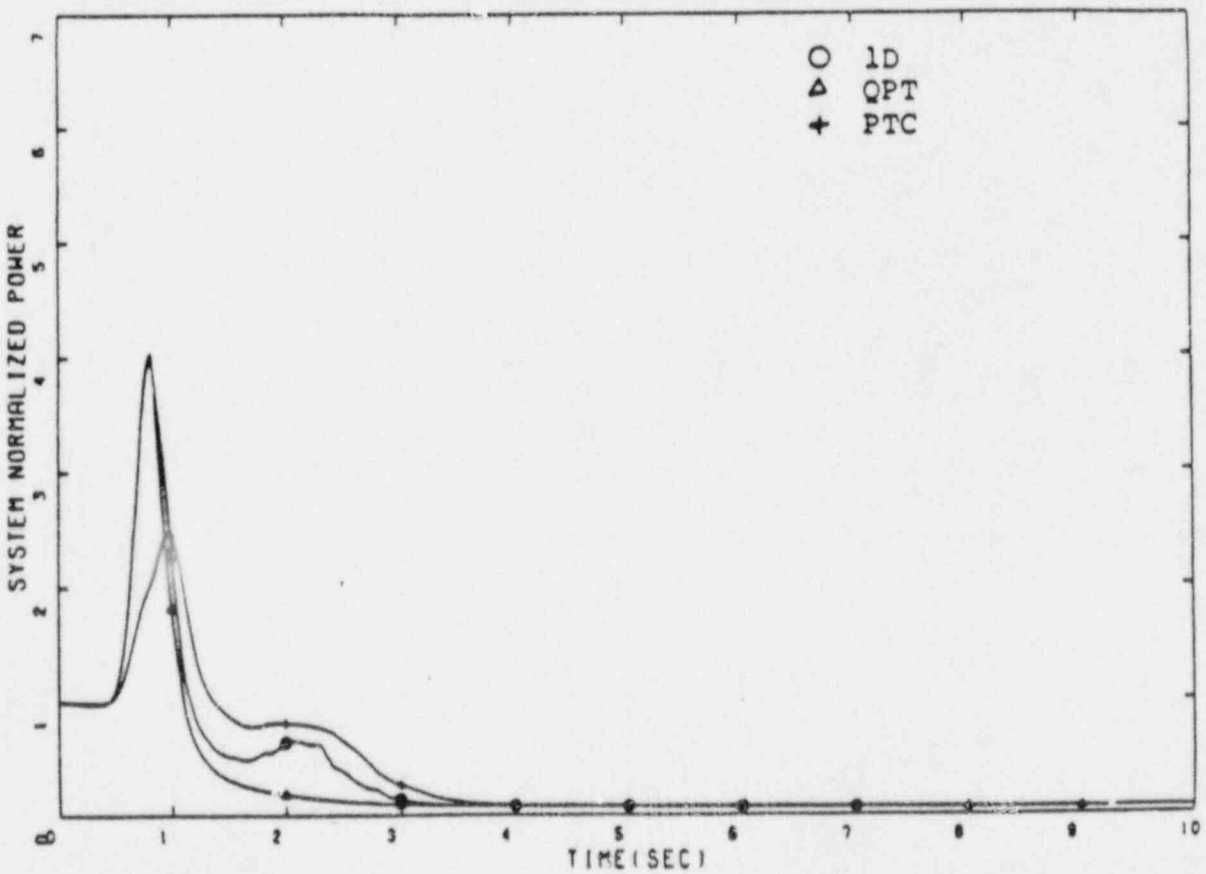

Figure 12 Comparison of System Normalized Power During TT1

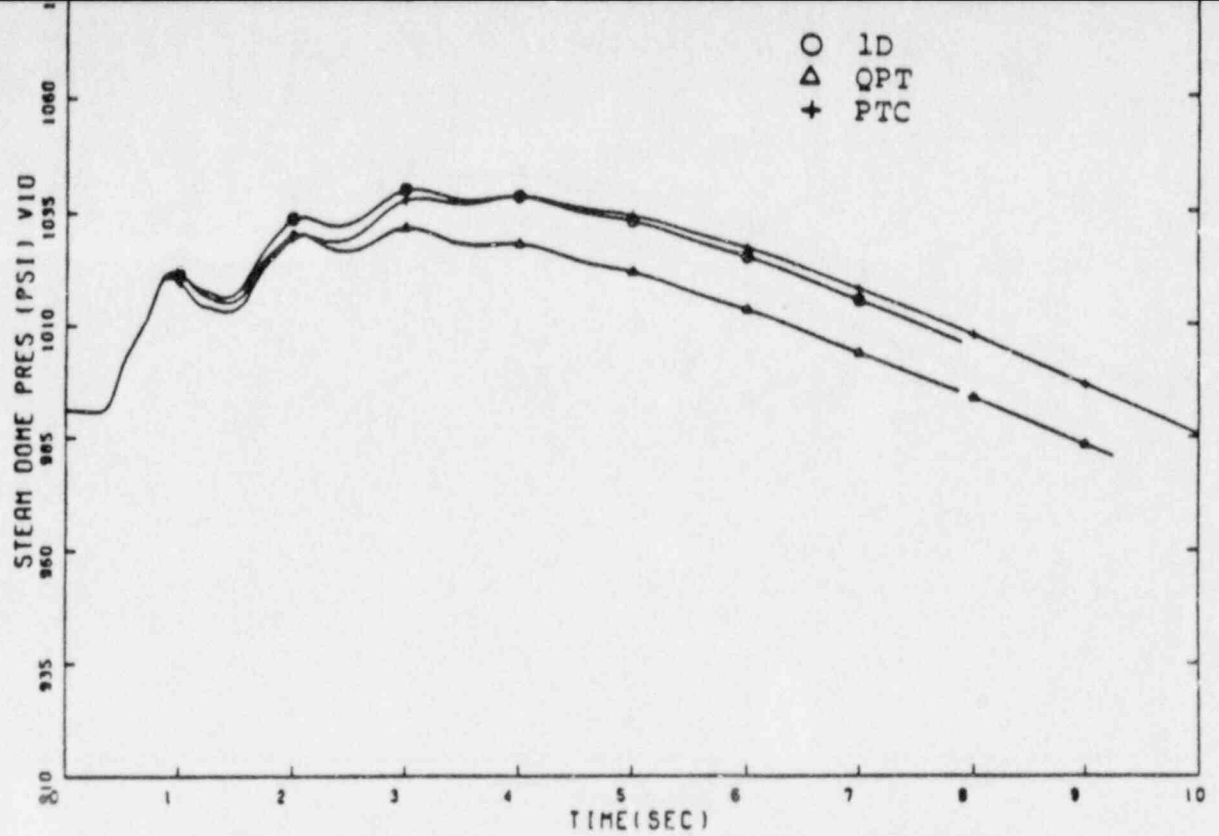

Figure 13 Comparison of Steam Dome Pressure During TT1

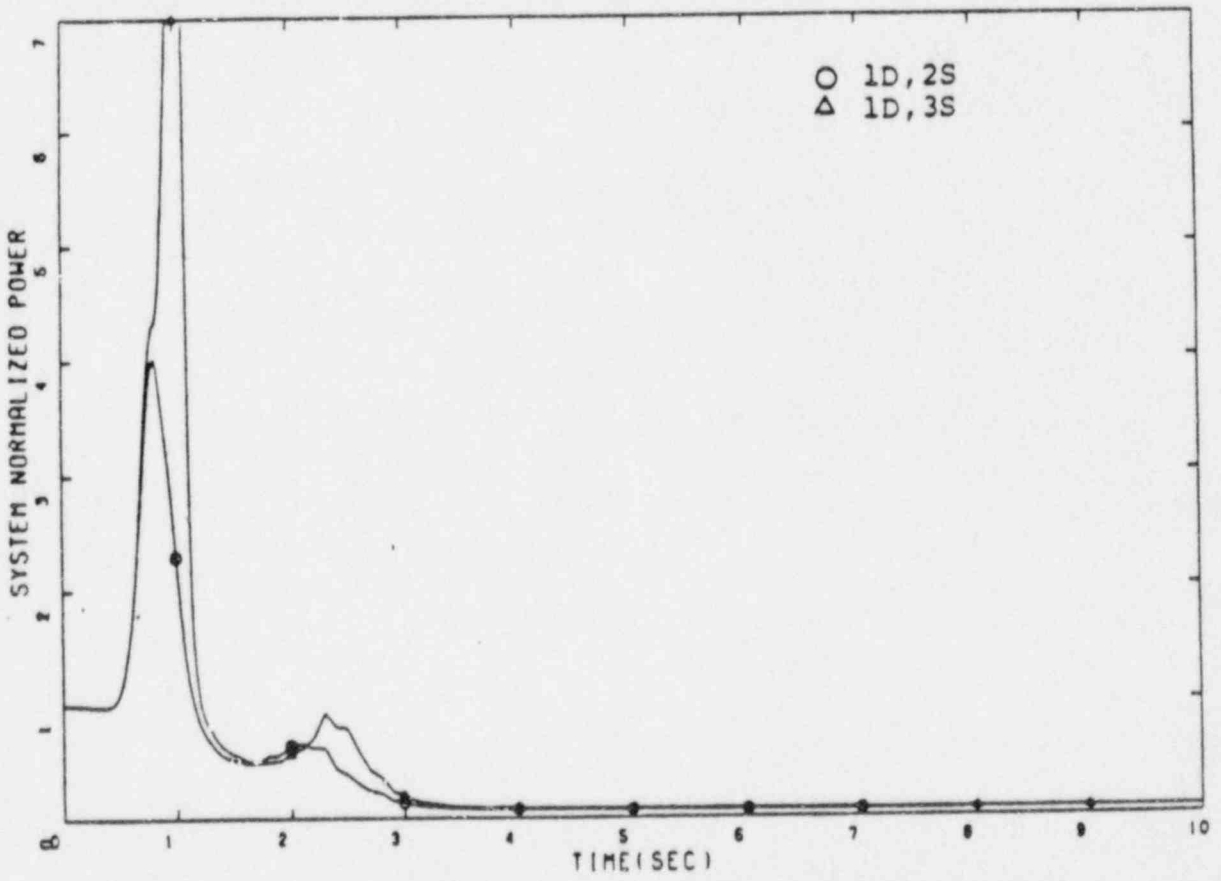

Figure 14 Comparison of Power Calculated By One-Dimensional Kinetics Using the 2S and 3S Cross-Section Sets for TT1

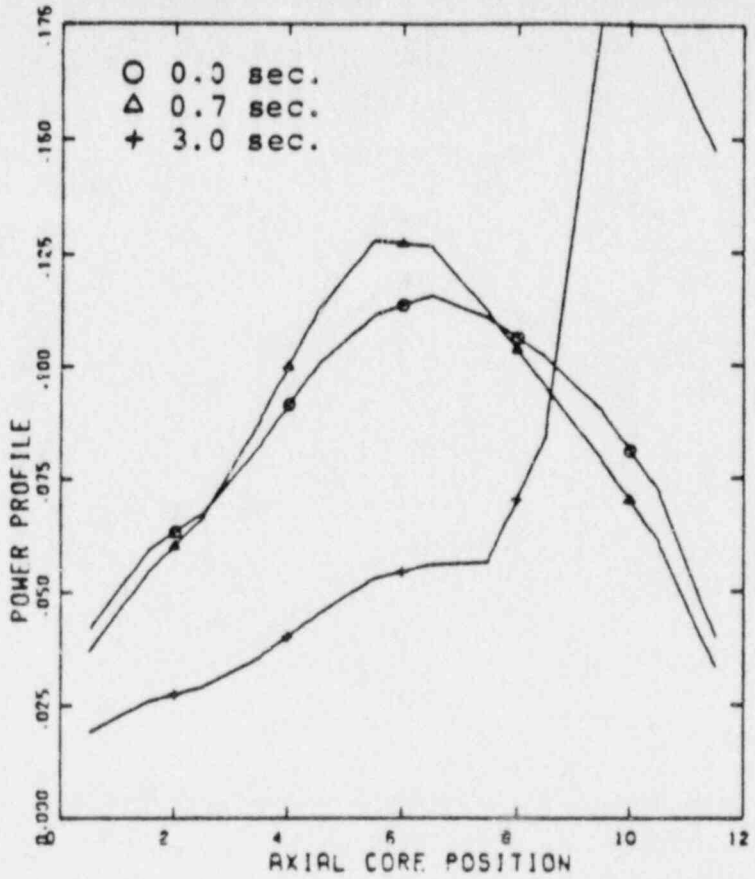

Figure 15 Axial Power Profiles During TT2

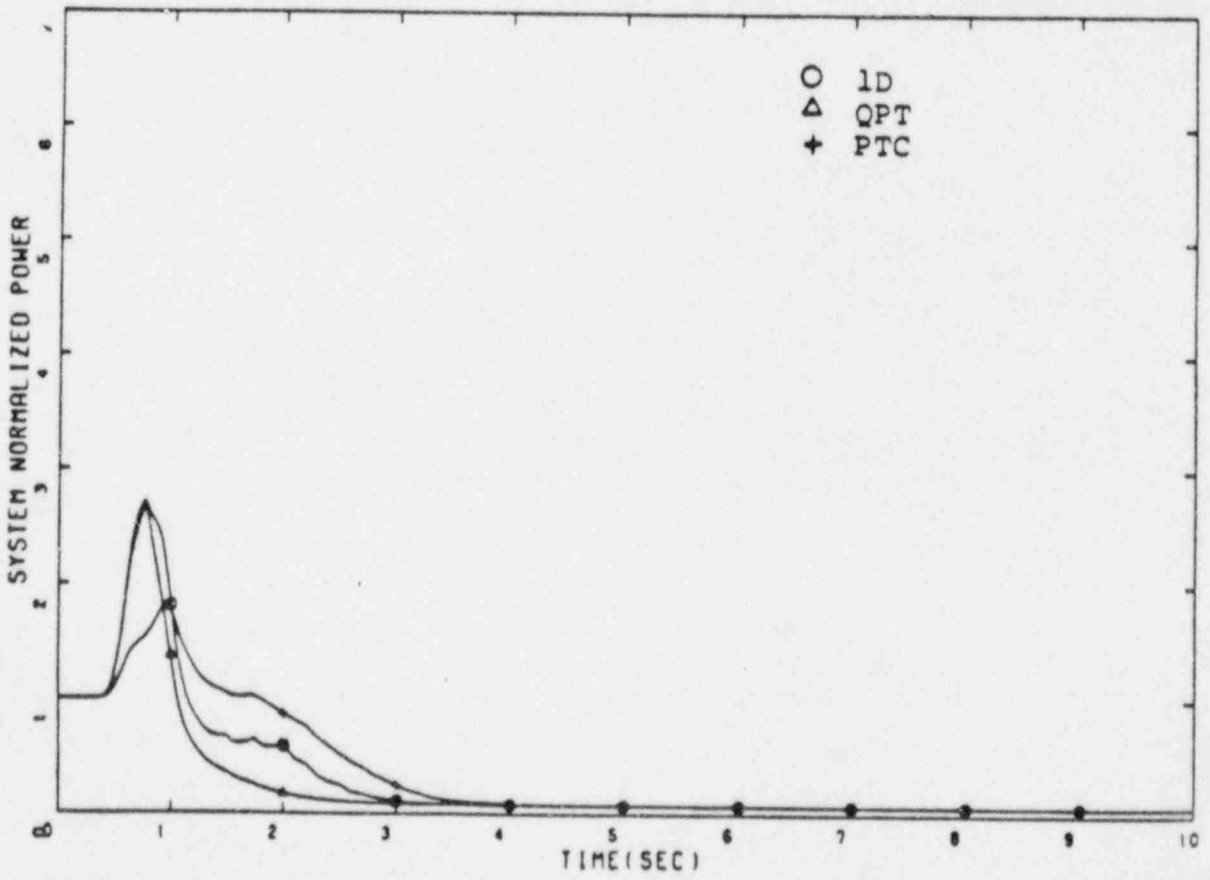

Figure 16 Comparison of System Normalized Power During TT2

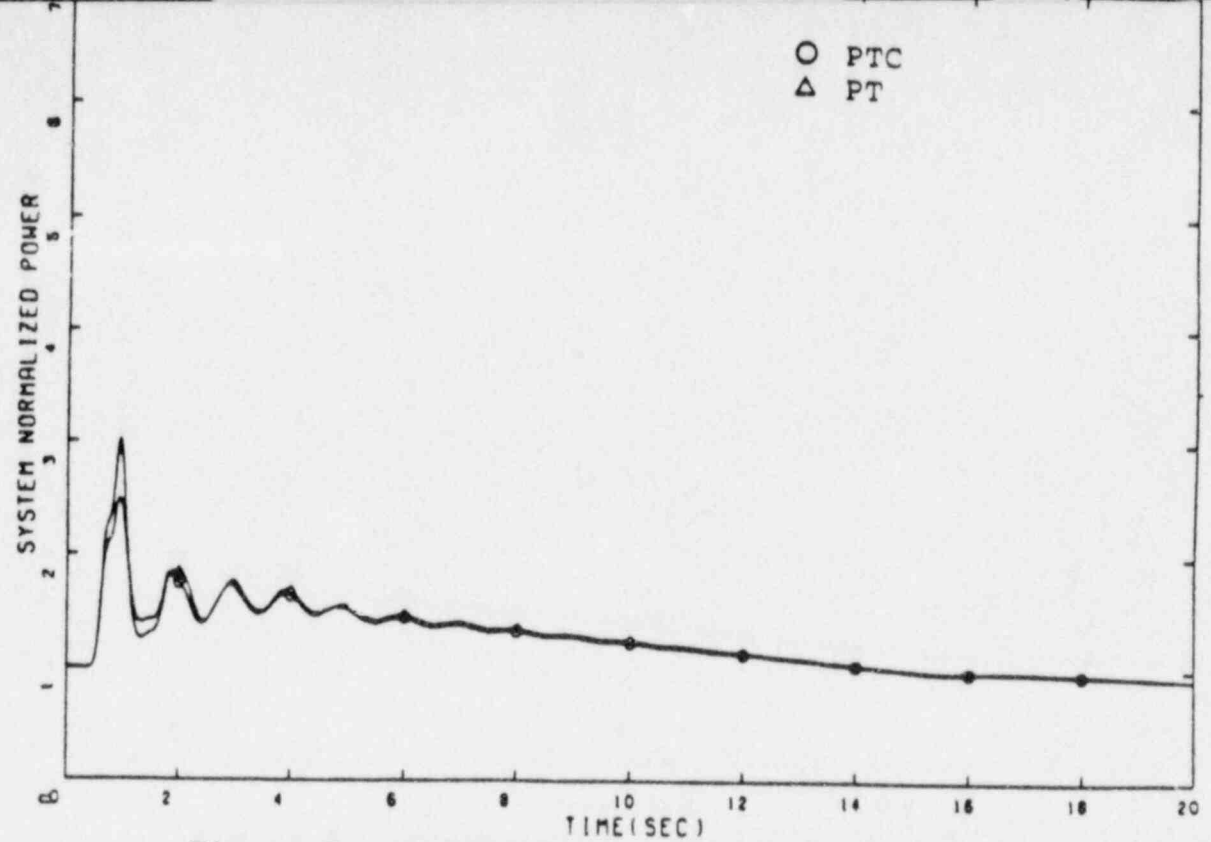

Figure 5: Comparison of System Normalized Power Using Core Averaged and Volume Averaged Quantities

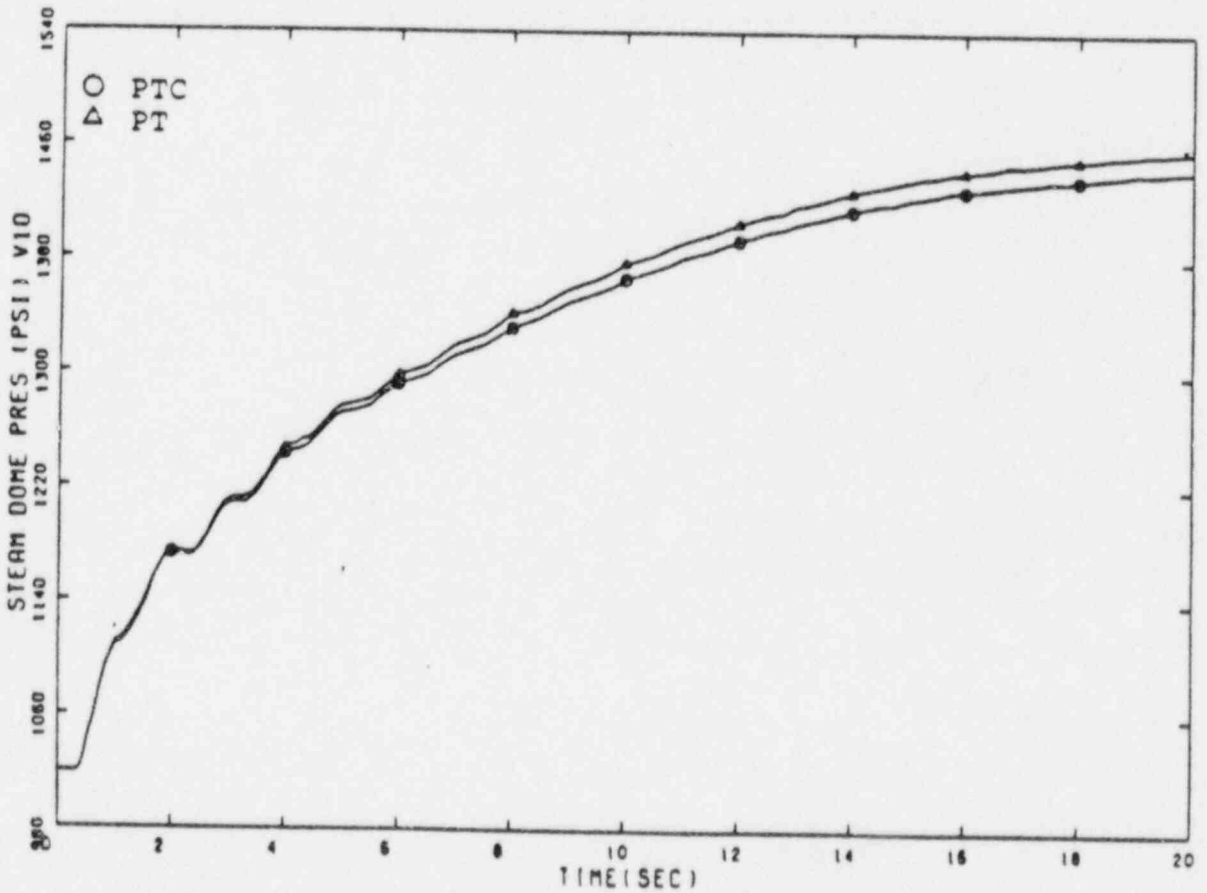

Figure 6 Comparison of Steam Dome Pressure Using Core Averaged and Volume Averaged Quantities

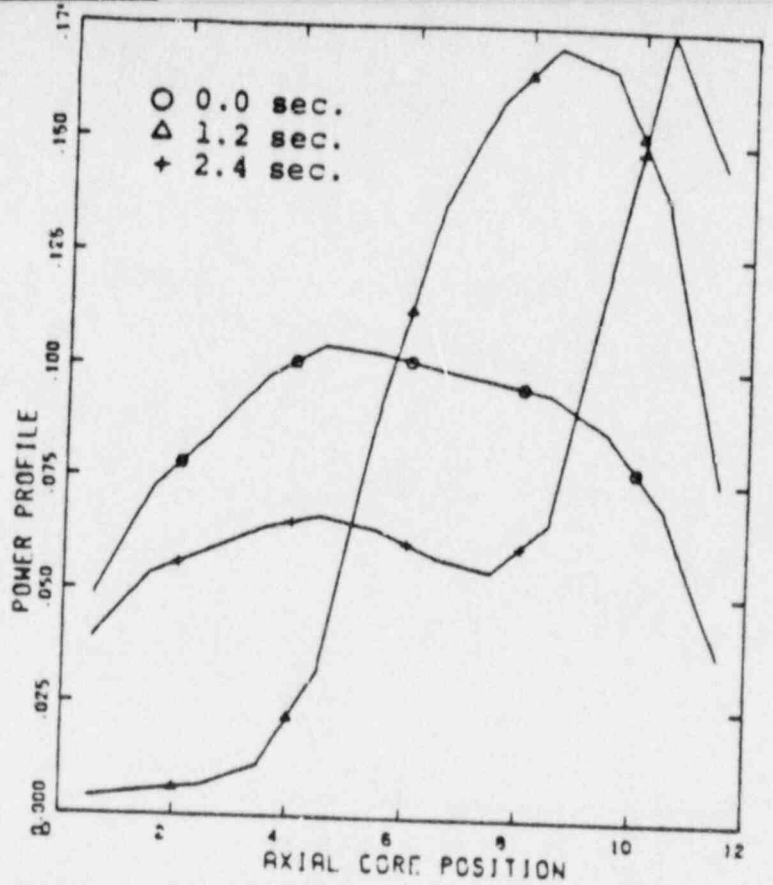

Figure 7 Axial Power Profiles During Scram Transient

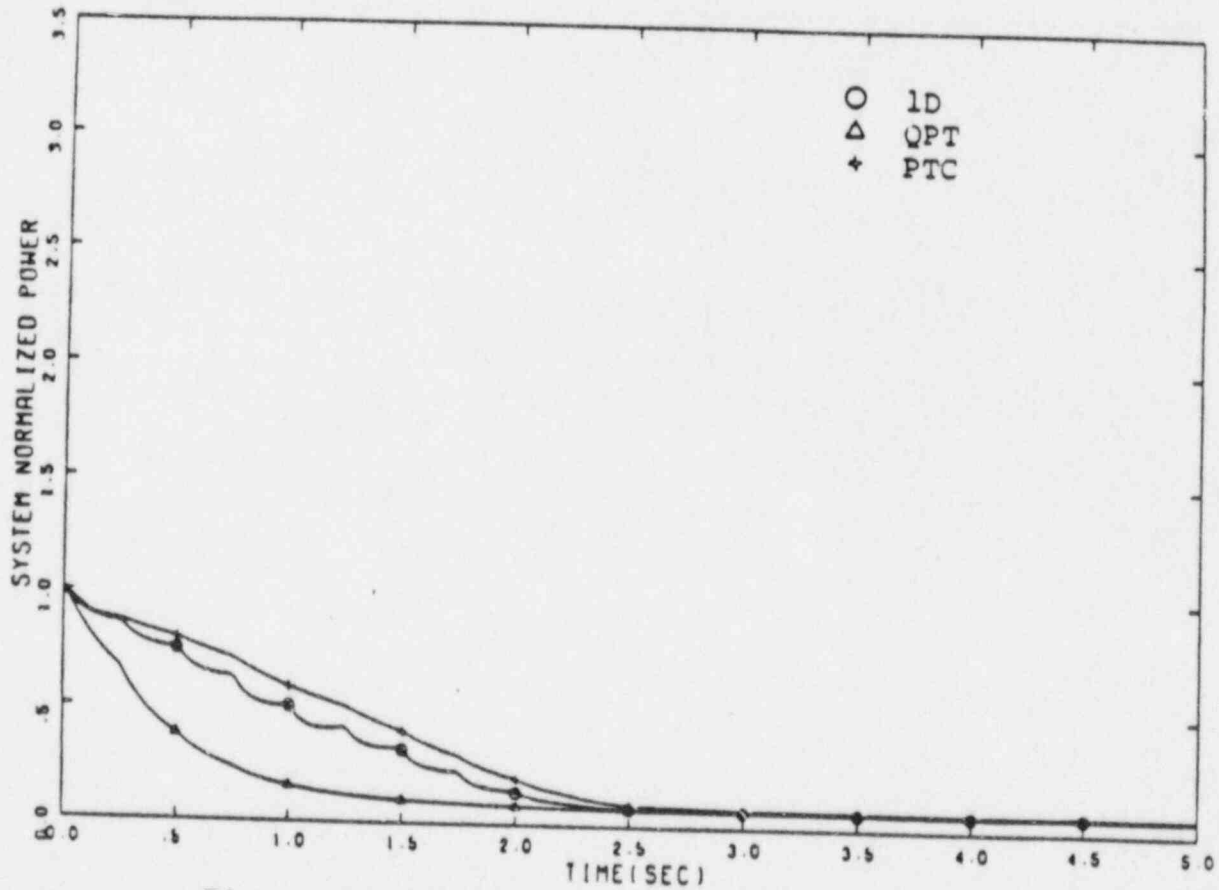

Figure 8 Comparison of System Normalized Power During Scram Transient

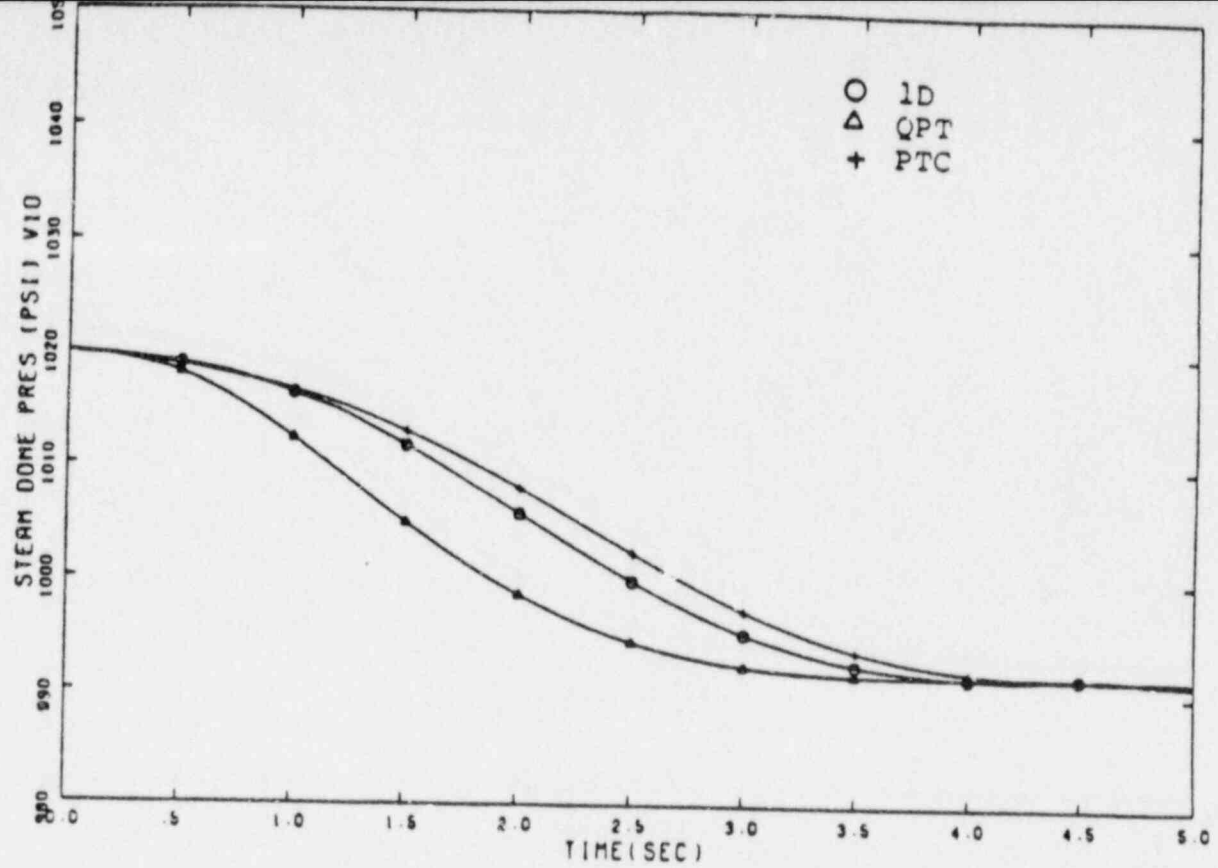

Figure 9 Comparison of Steam Dome Pressure During Scram Transient

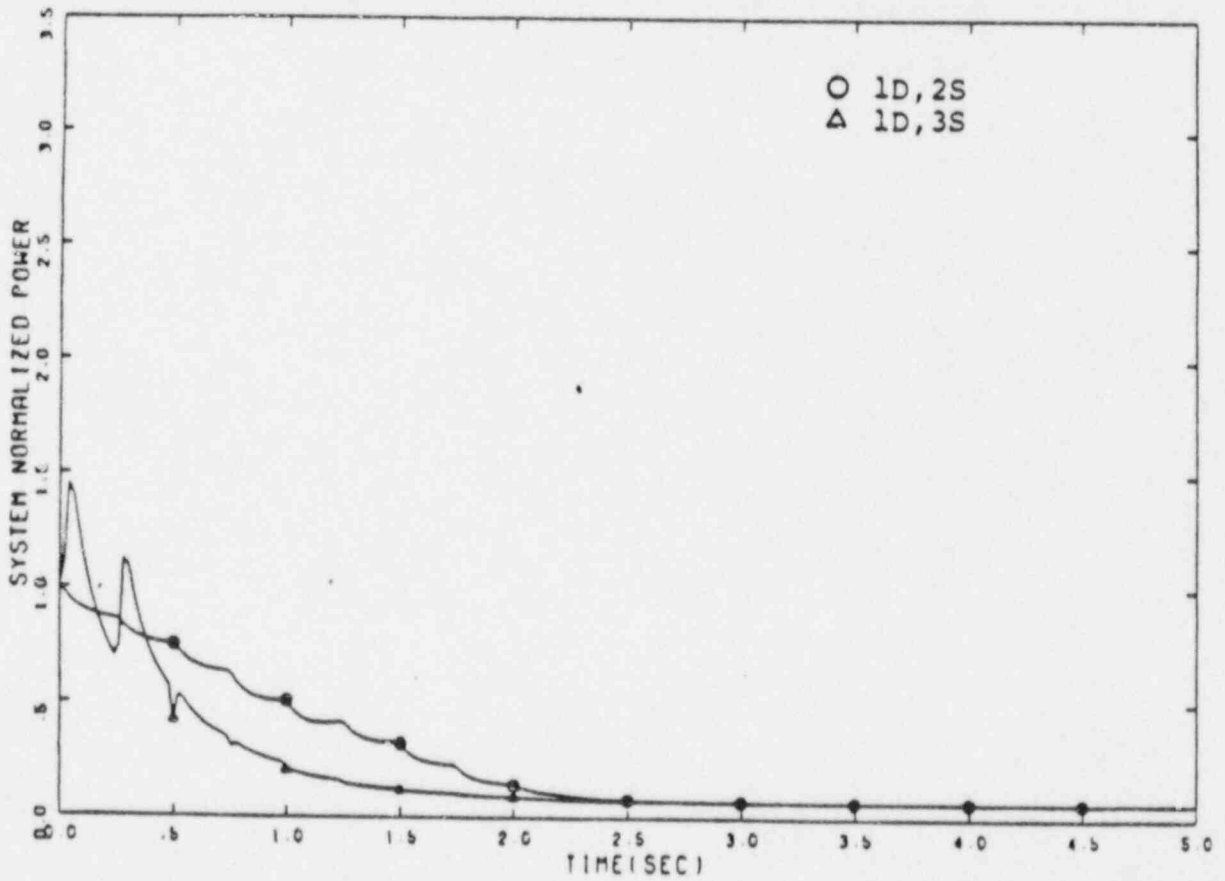

Figure 10 Comparison of Power Calculated by One-Dimensional Kinetics Using the 2S and 3S Cross-Section Sets for the Scram Transient

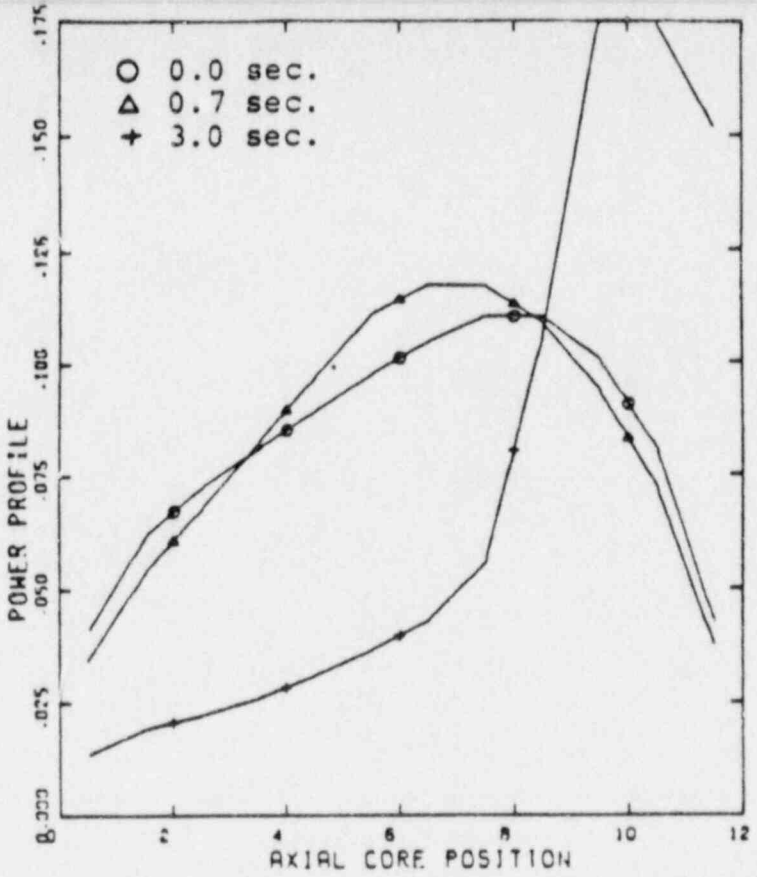

Figure 11 Axial Power Profiles During TT1

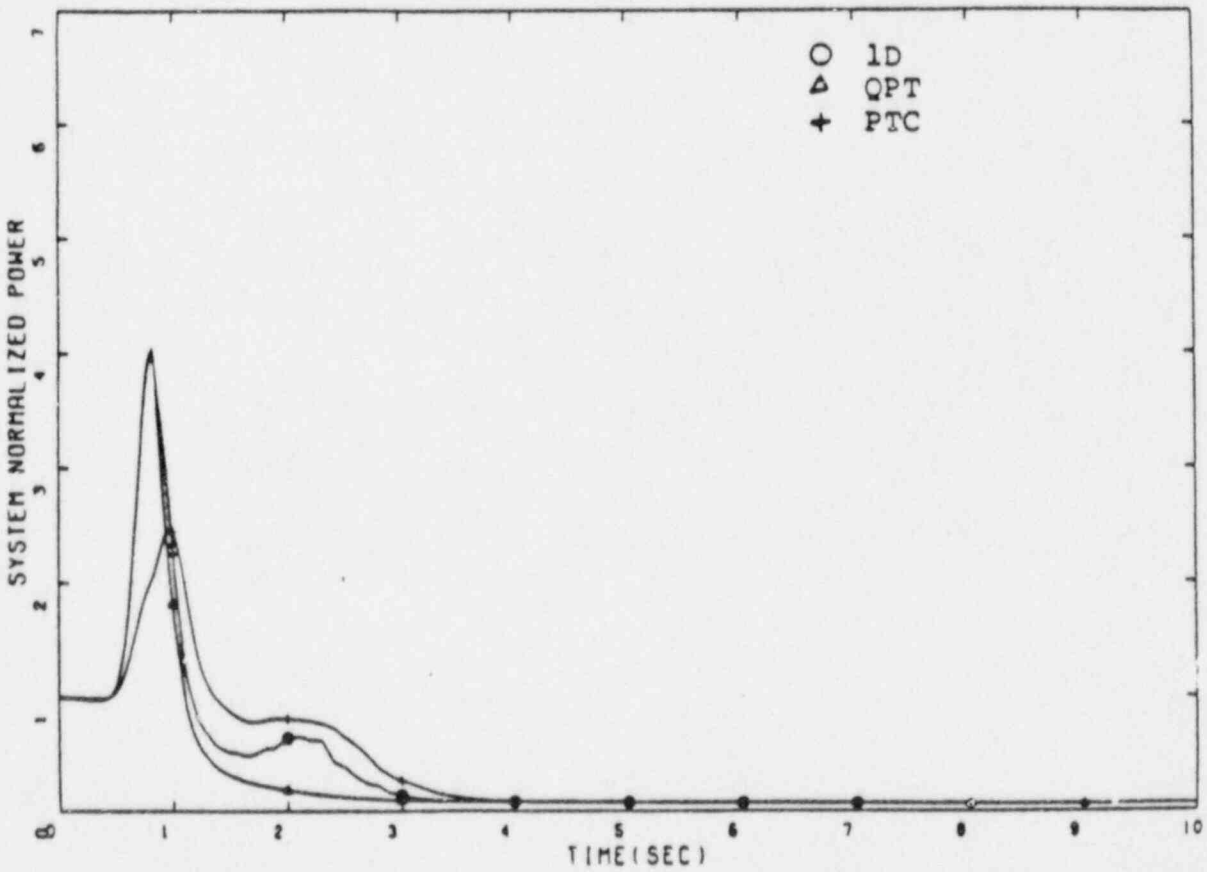

Figure 12 Comparison of System Normalized Power During TT1

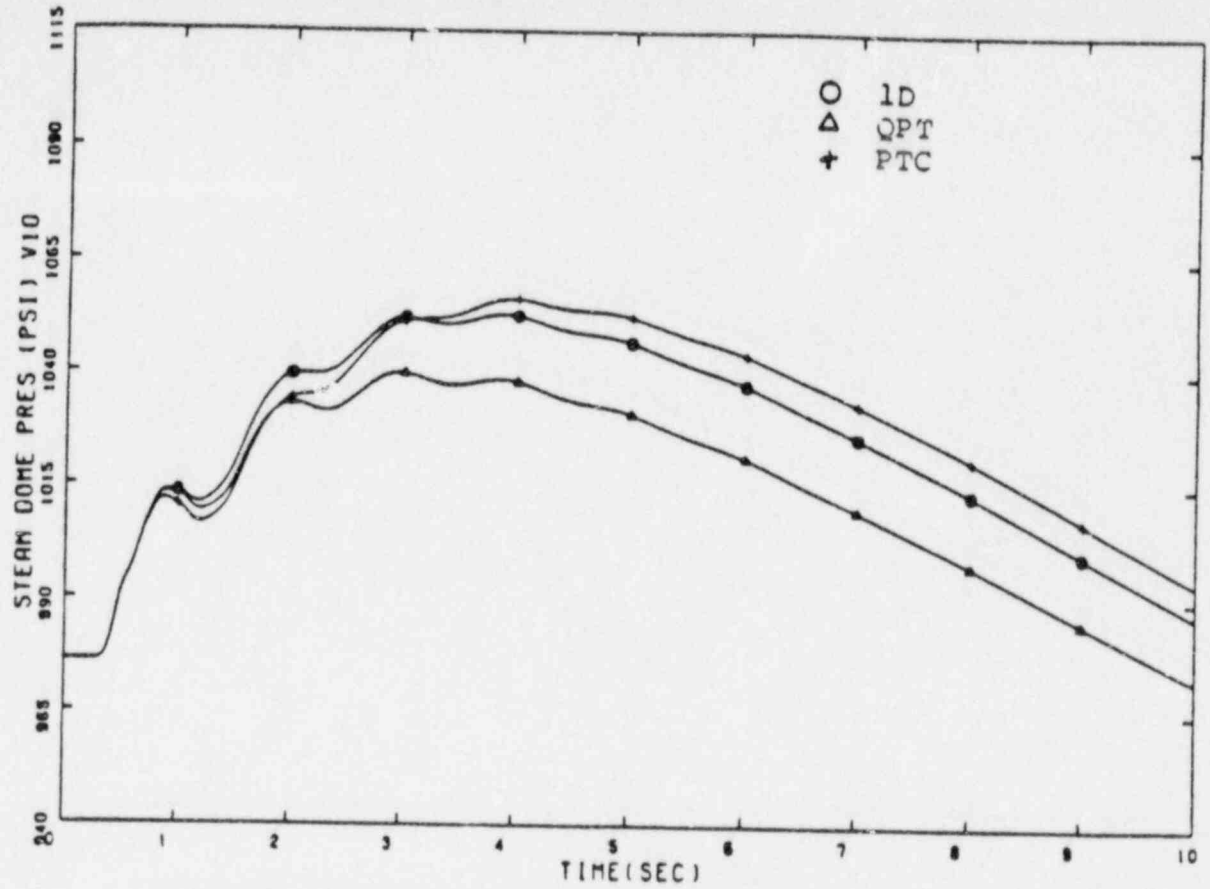

Figure 17 Comparison of Steam Dome Pressure During TT2

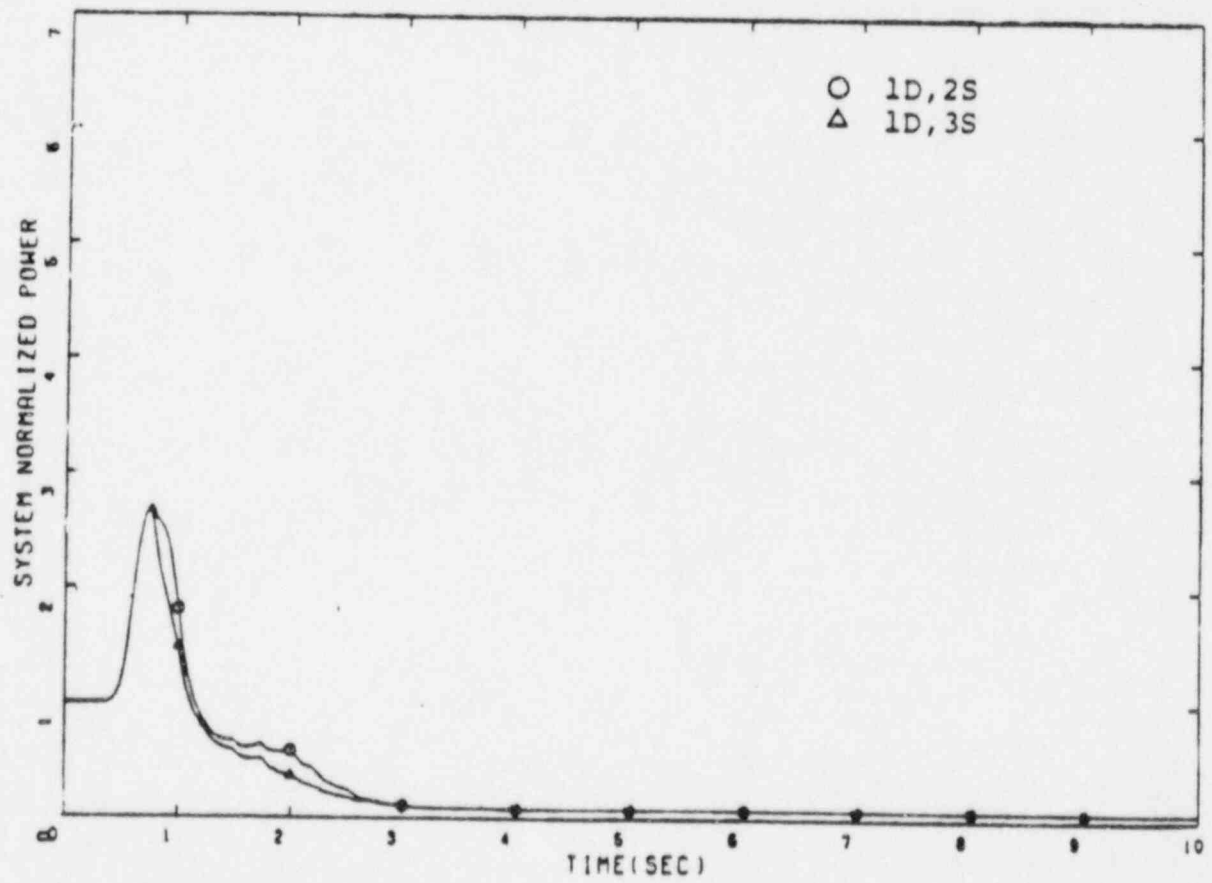

Figure 18 Comparison of Power Calculated By One-Dimensional Kinetics Using the 2S and 3S Cross-Section Sets for TT2

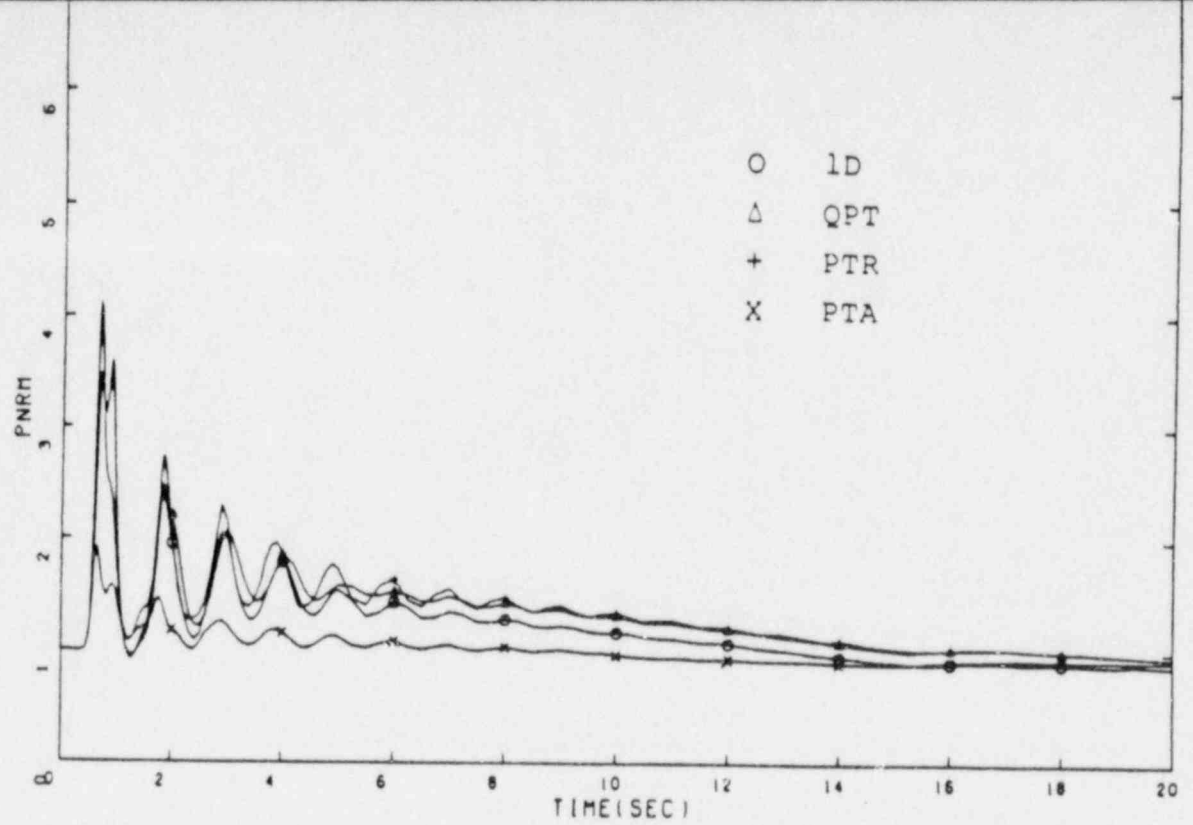

Figure 19 Comparison of System Normalized Power During ATWS

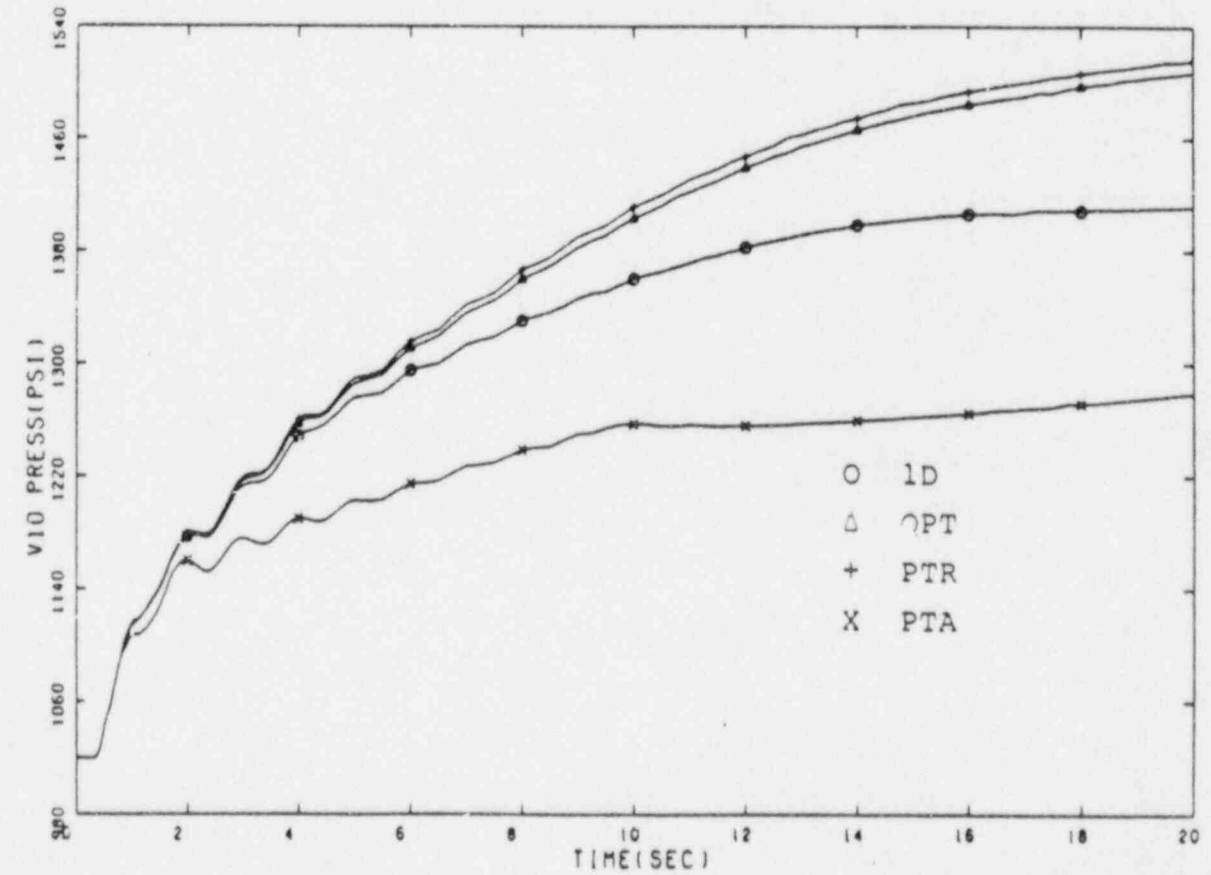

Figure 20 Comparison of Steam Dome Pressure During ATWS

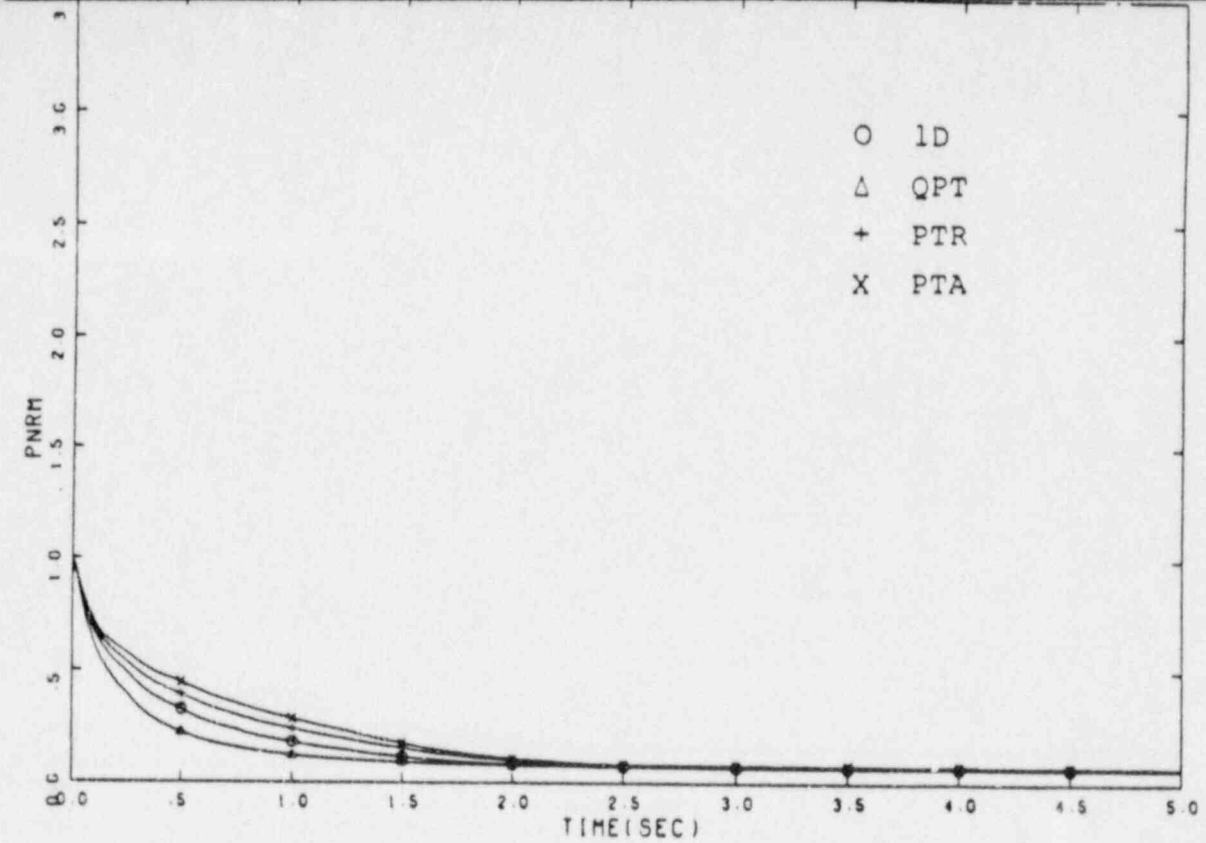

Figure 21 Comparison of System Normalized Power During Scram Transient

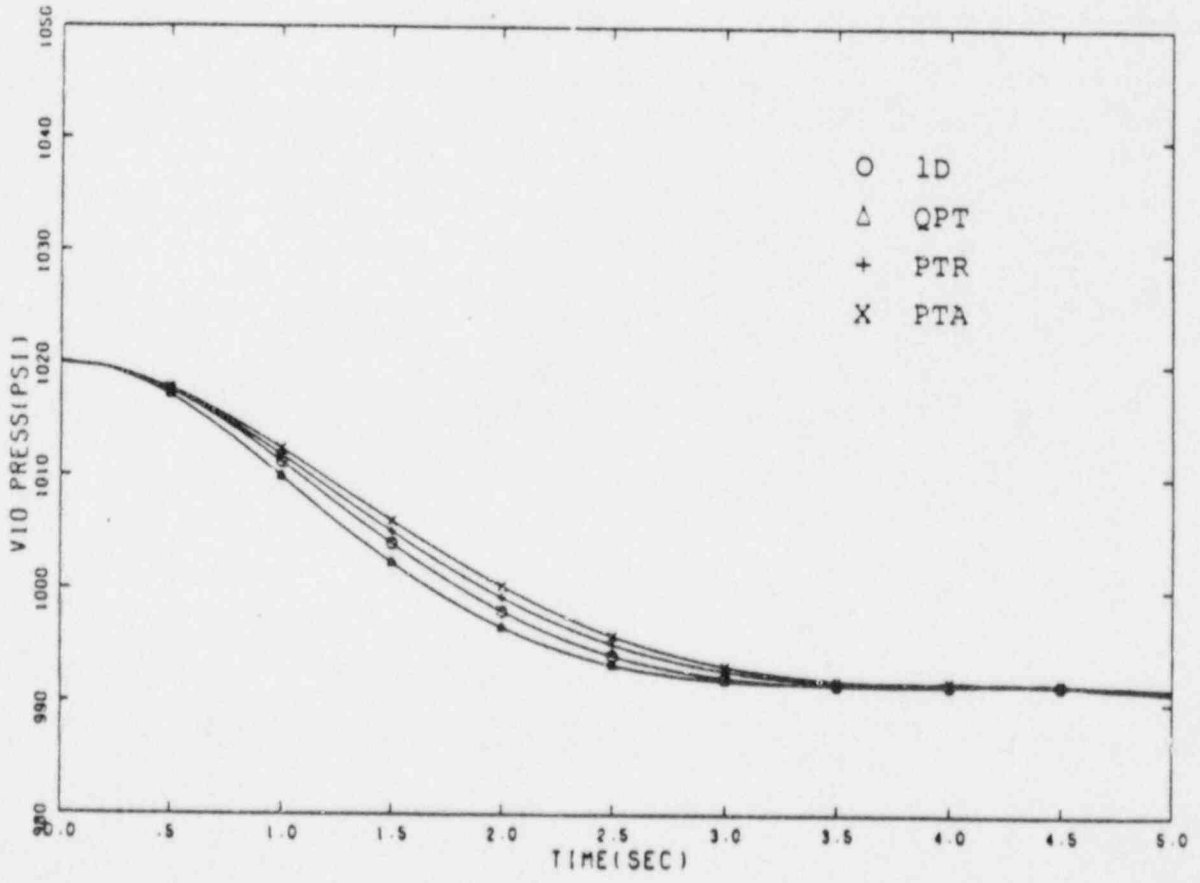

Figure 22 Comparison of Steam Dome Pressure During Scram Transient

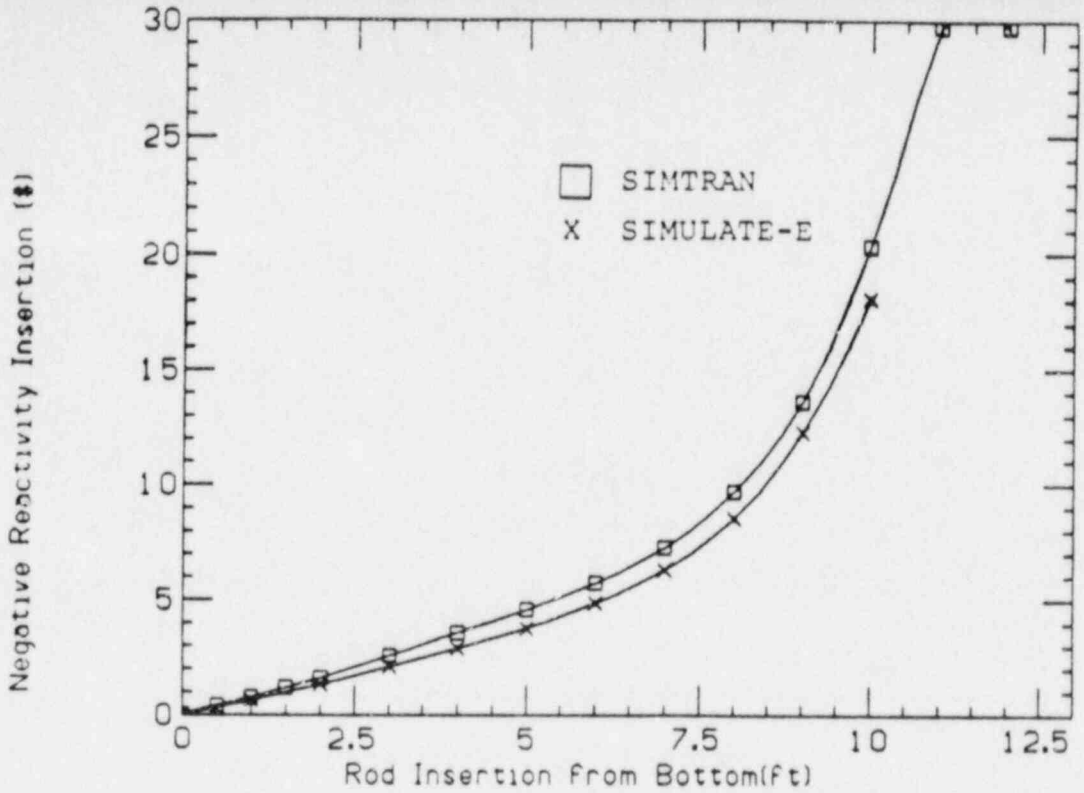

Figure 23 Comparison of Scram Curve Calculated by SIMULATE-E and SIMTRAN for TT1

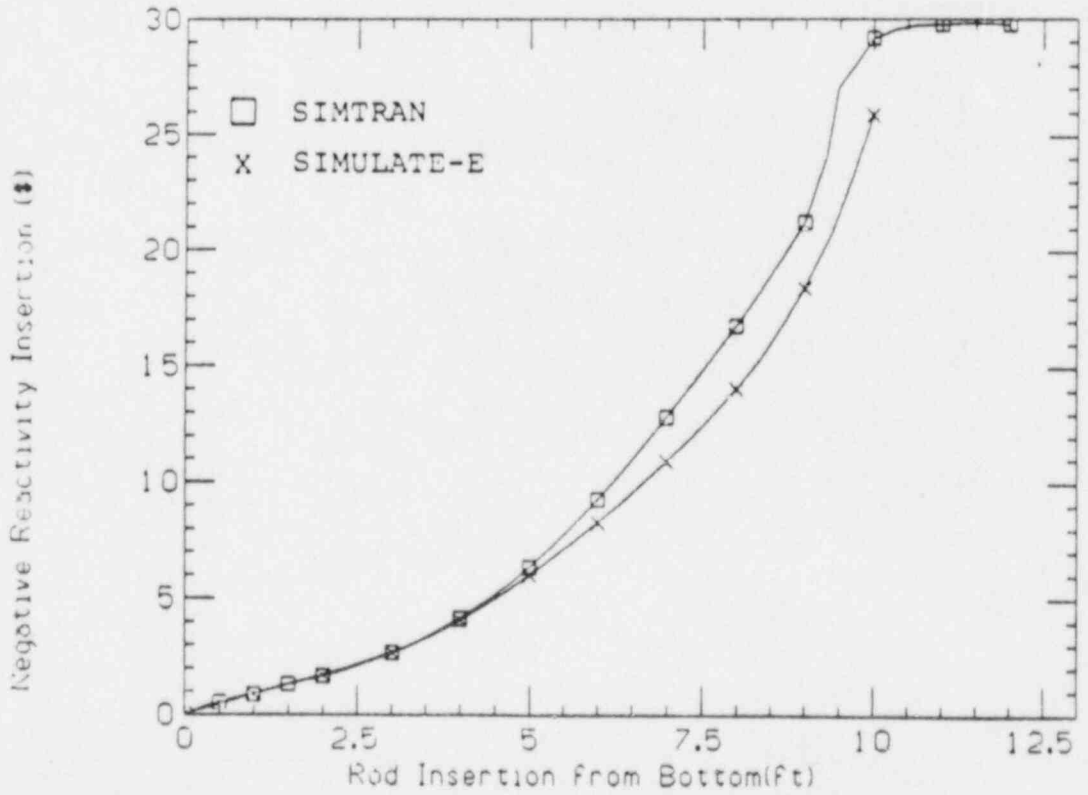

Figure 24 Comparison of Scram Curve Calculated by SIMULATE-E and SIMTRAN for TT2

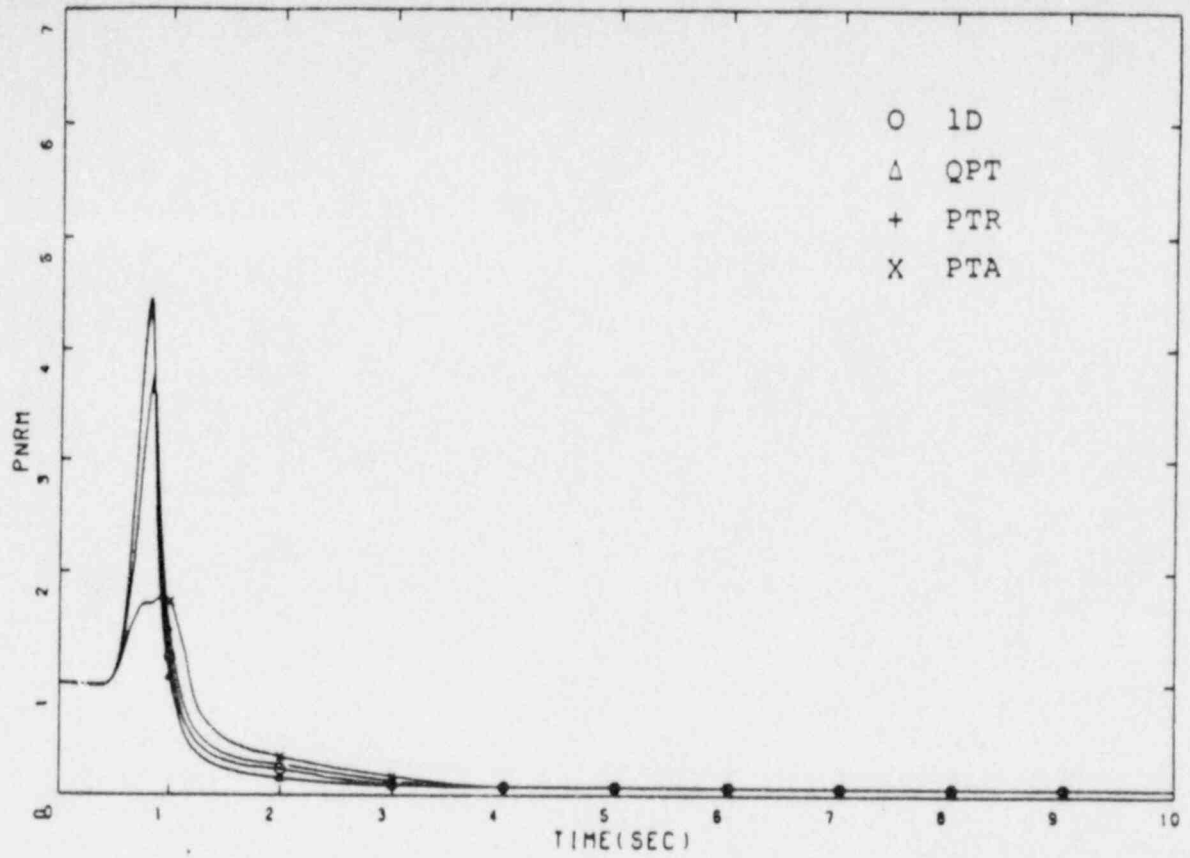

Figure 25 Comparison of System Normalized Power During TT1

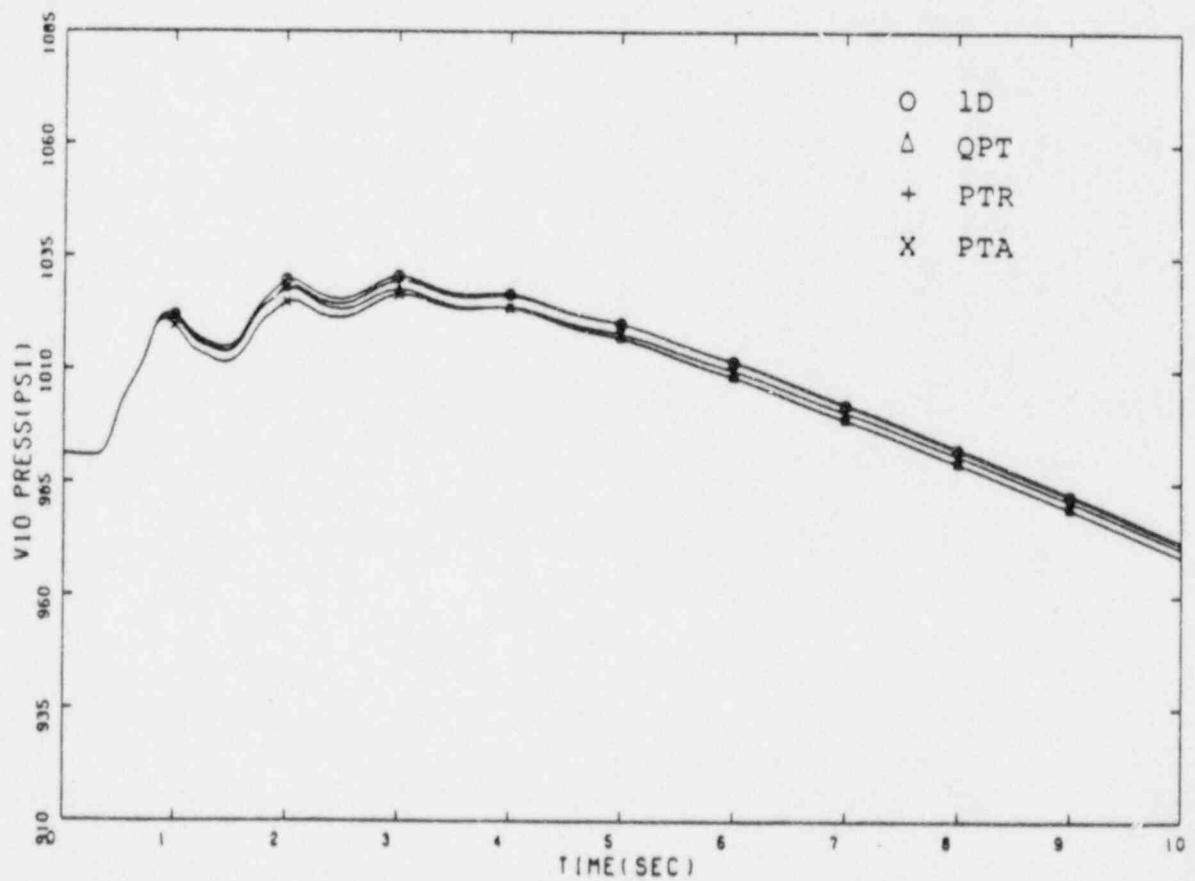

Figure 26 Comparison of Steam Dome Pressure During TT1

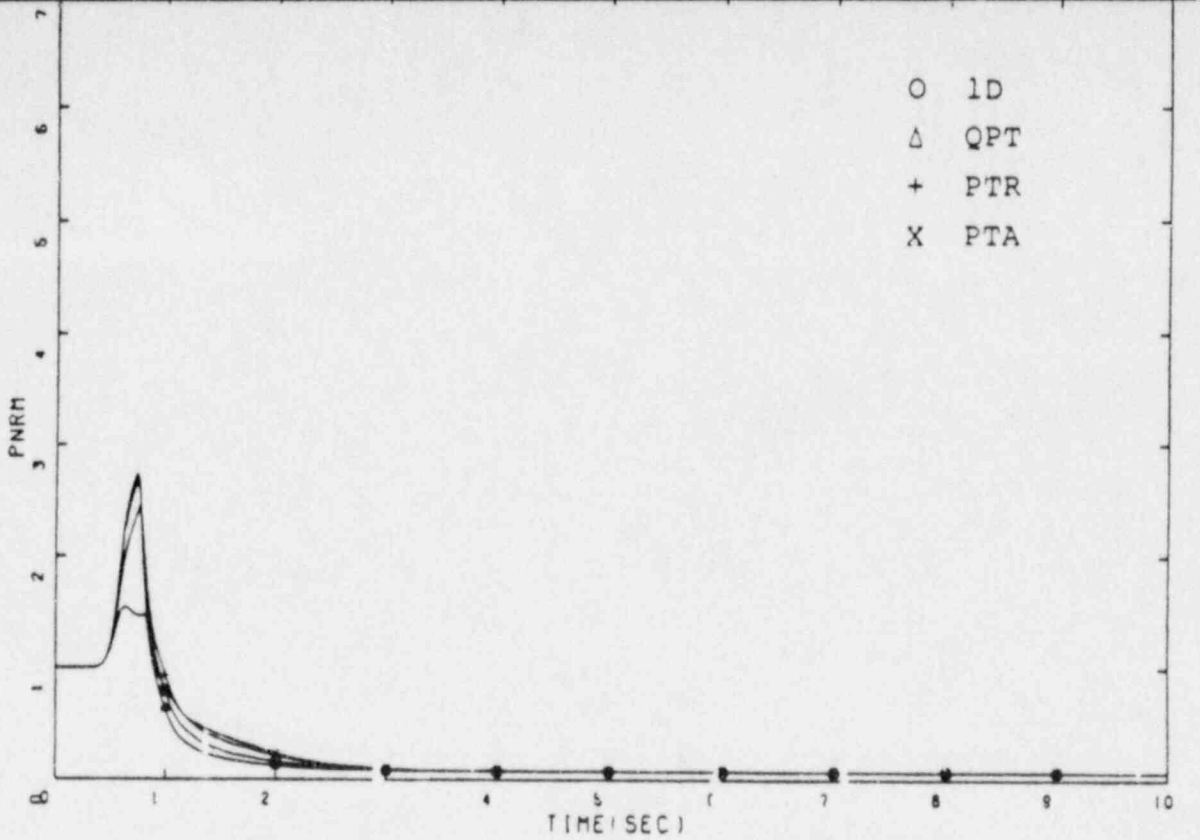

Figure 27 Comparison of System Normalized Power During TT2

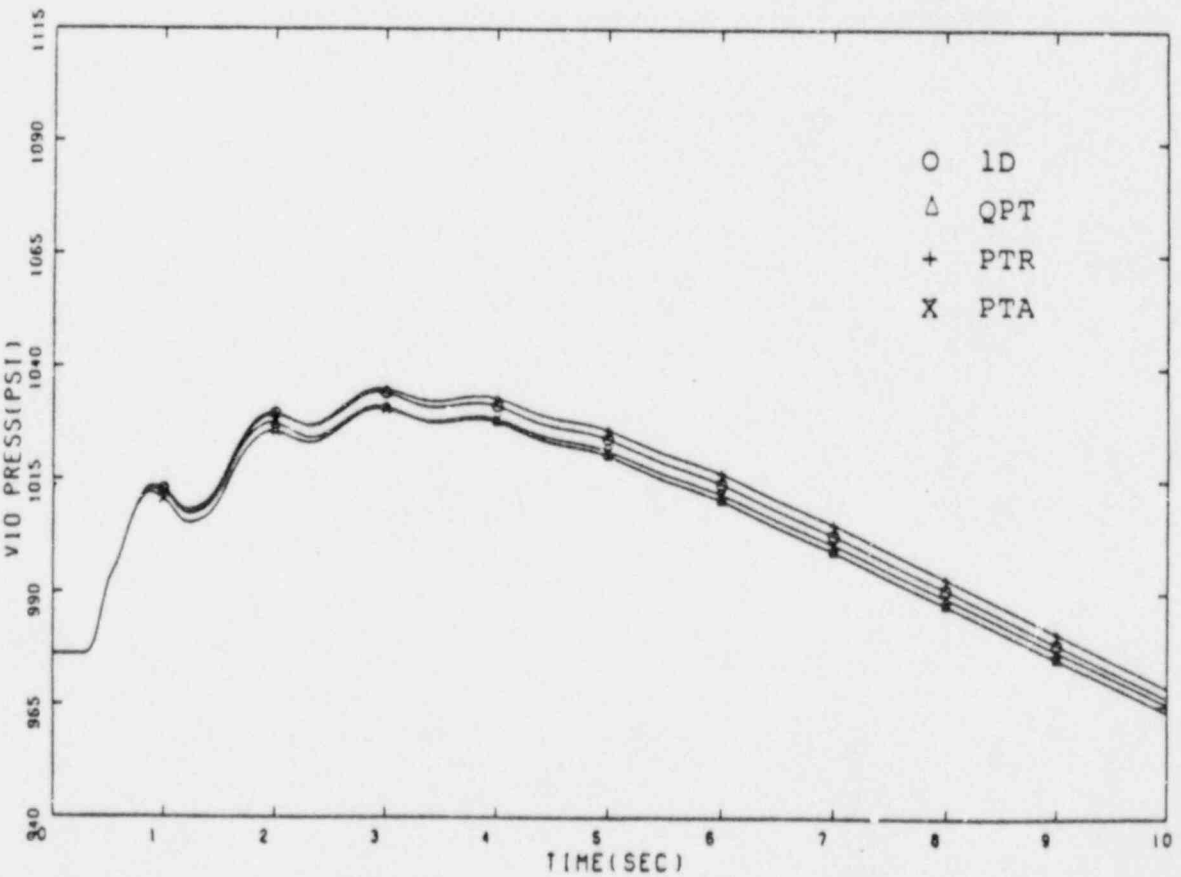

Figure 28 Comparison of Steam Dome Pressure During TT2

All Rods Out (ARO)

1.893 1.925					
1.865 1.896	1.838 1.867				
1.782 1.808	1.754 1.780	1.671 1.692			
1.639 1.659	1.612 1.630	1.529 1.542	1.387 1.393		
1.432 1.442	1.405 1.414	1.323 1.327	1.183 1.181	0.982 0.973	
1.155 1.153	1.130 1.127	1.051 1.044	0.915 0.904	0.719 0.706	0.482 0.469
0.802 0.791	0.782 0.770	0.711 0.698	0.584 0.570	0.388 0.376	0.200 0.193
0.368 0.358	0.368 0.352	0.312 0.302	0.221 0.213		

NODE-P2 k-eff
1.0389
SIMULATE-E k-eff
1.0425

All Rods In (ARI)

1.366 1.365					
2.217 2.217	2.583 2.592				
1.331 1.332	2.195 2.200	1.405 1.409			
2.042 2.049	2.454 2.472	2.378 2.395	2.373 2.393		
0.937 0.937	1.720 1.728	1.989 2.002	1.621 1.628	0.640 0.637	
0.614 0.605	0.561 0.557	0.966 0.963	0.513 0.510	0.460 0.451	0.362 0.351
0.226 0.219	0.346 0.338	0.271 0.266	0.291 0.284	0.134 0.130	0.128 0.123
0.163 0.156	0.195 0.187	0.157 0.151	0.128 0.123		

NODE-P2 k-eff
0.9700
SIMULATE-E k-eff
0.9723

NODE-P2 P(I,J)
SIMULATE-E P(I,J)

Figure 29 (a) Comparison of NODE-P2 and SIMULATE-E eigenvalue and relative power distribution by assembly

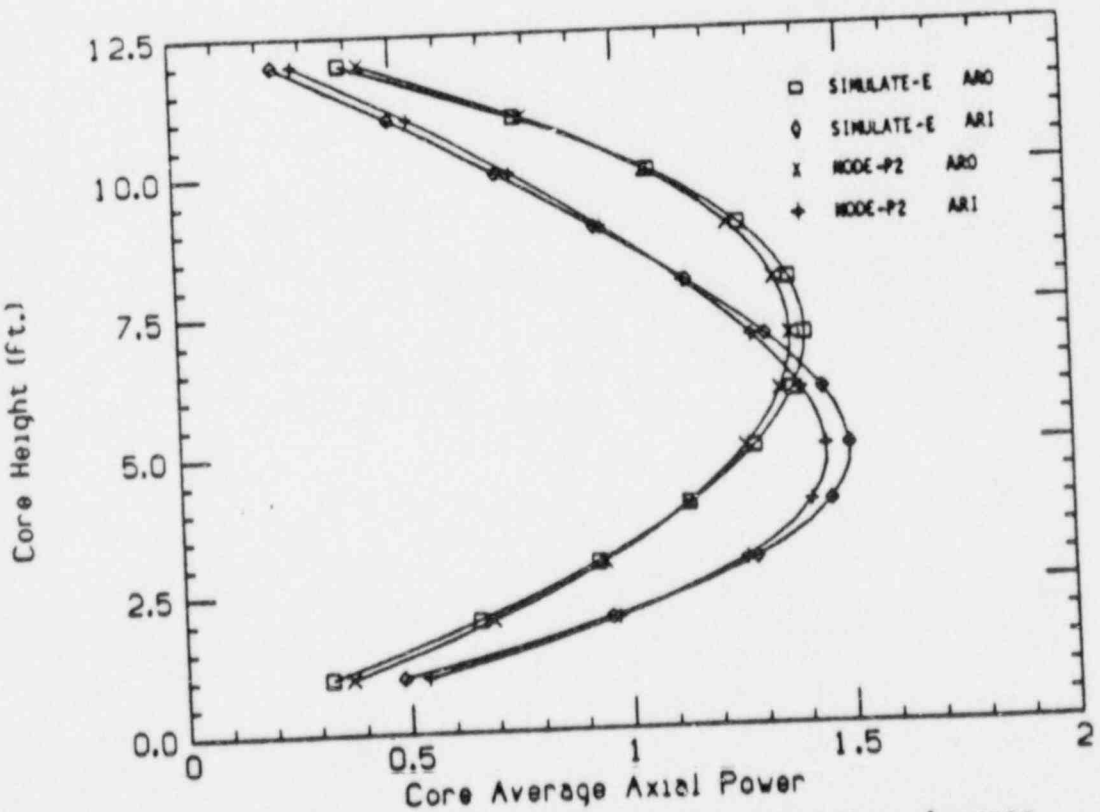

Figure 29 (b) Comparison of NODE-P2 and SIMULATE-E Core Average Axial Power

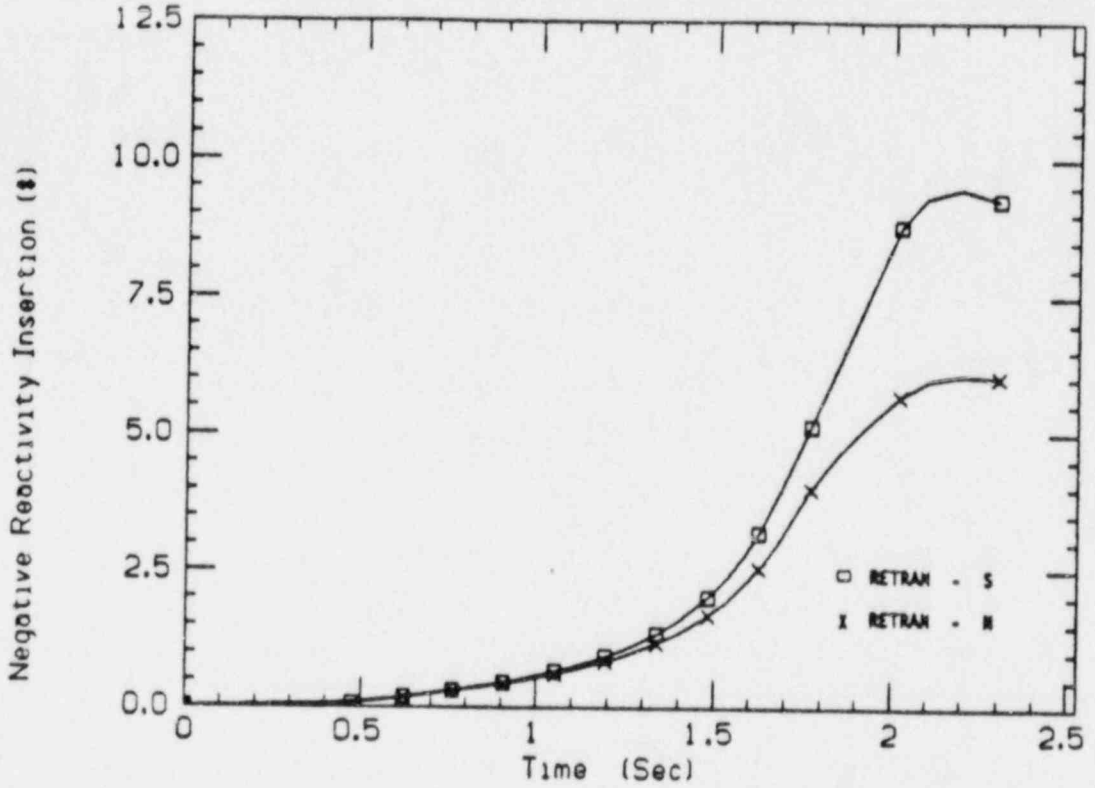

Figure 30 Comparison of RETRAN-N and RETRAN-S Scram Curves

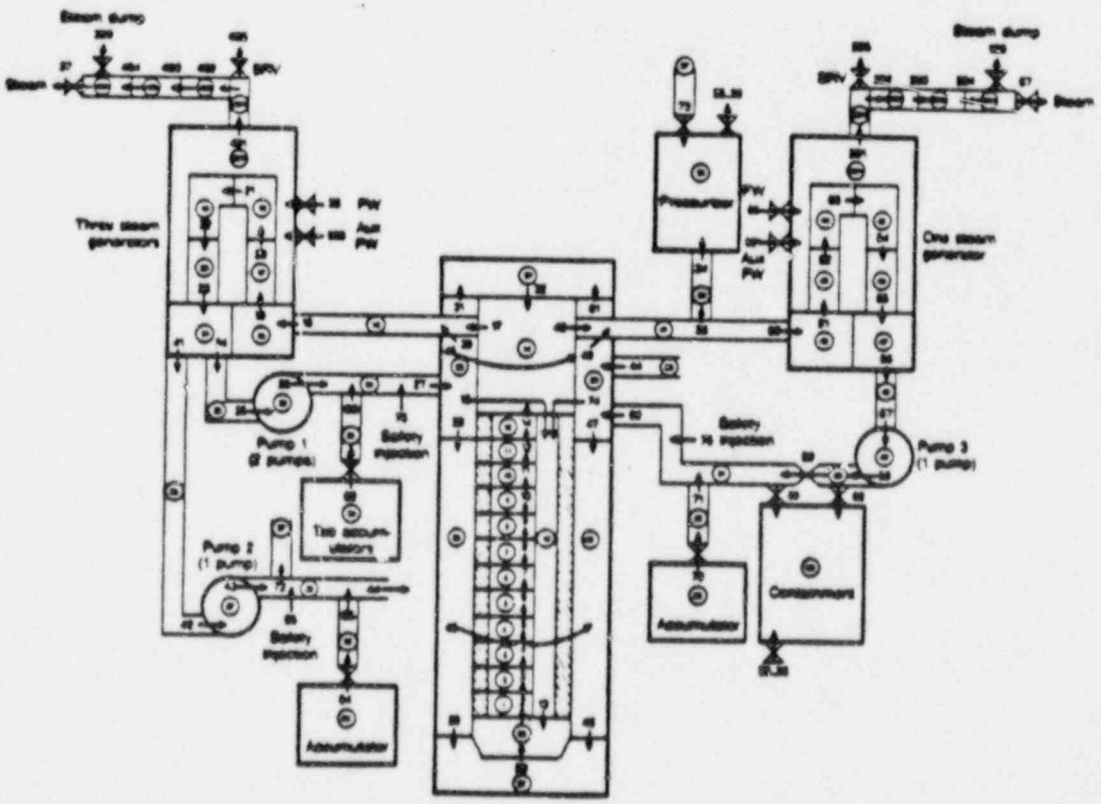

Figure 31 Schematic of PWR Plant Model

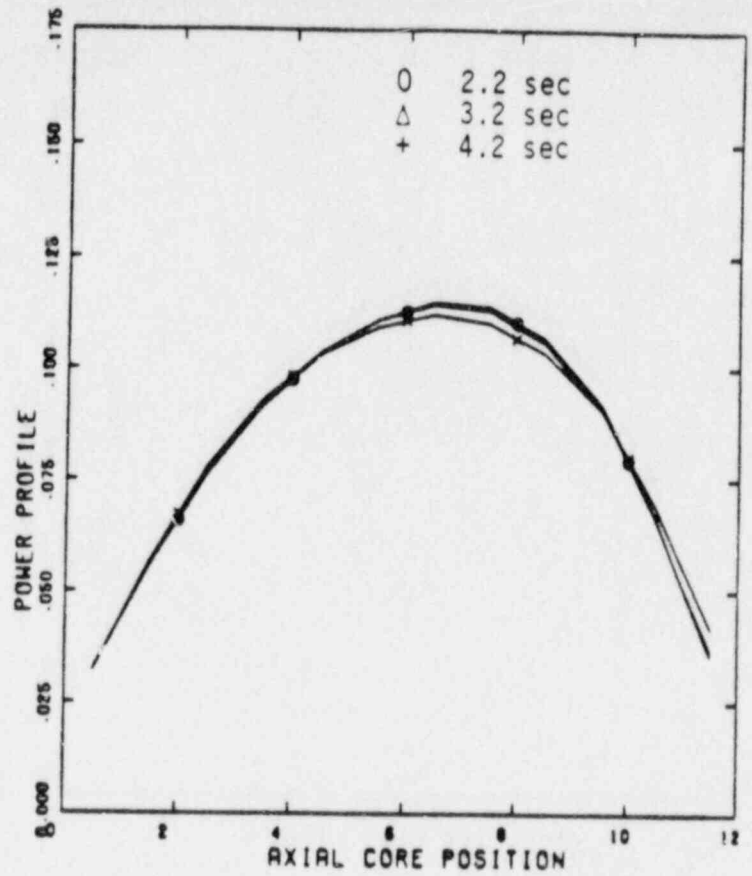

Figure 32 (a) Axial Power Profiles During ATWS (LOF) (RETRAN-N)

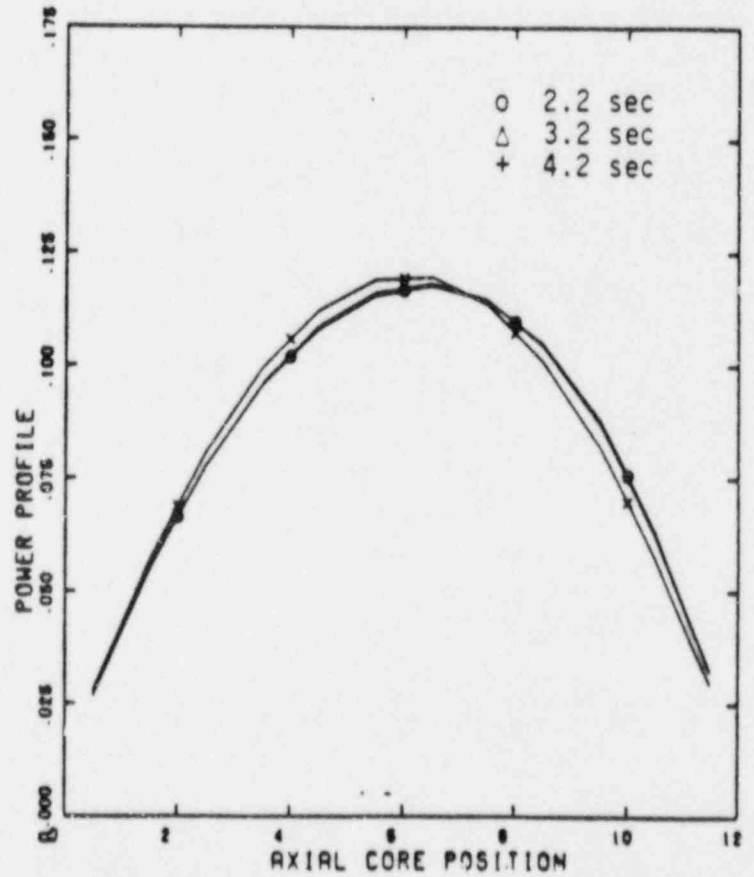

Figure 32 (b) Axial Power Profiles During ATWS (LOF) (RETRAN-S)

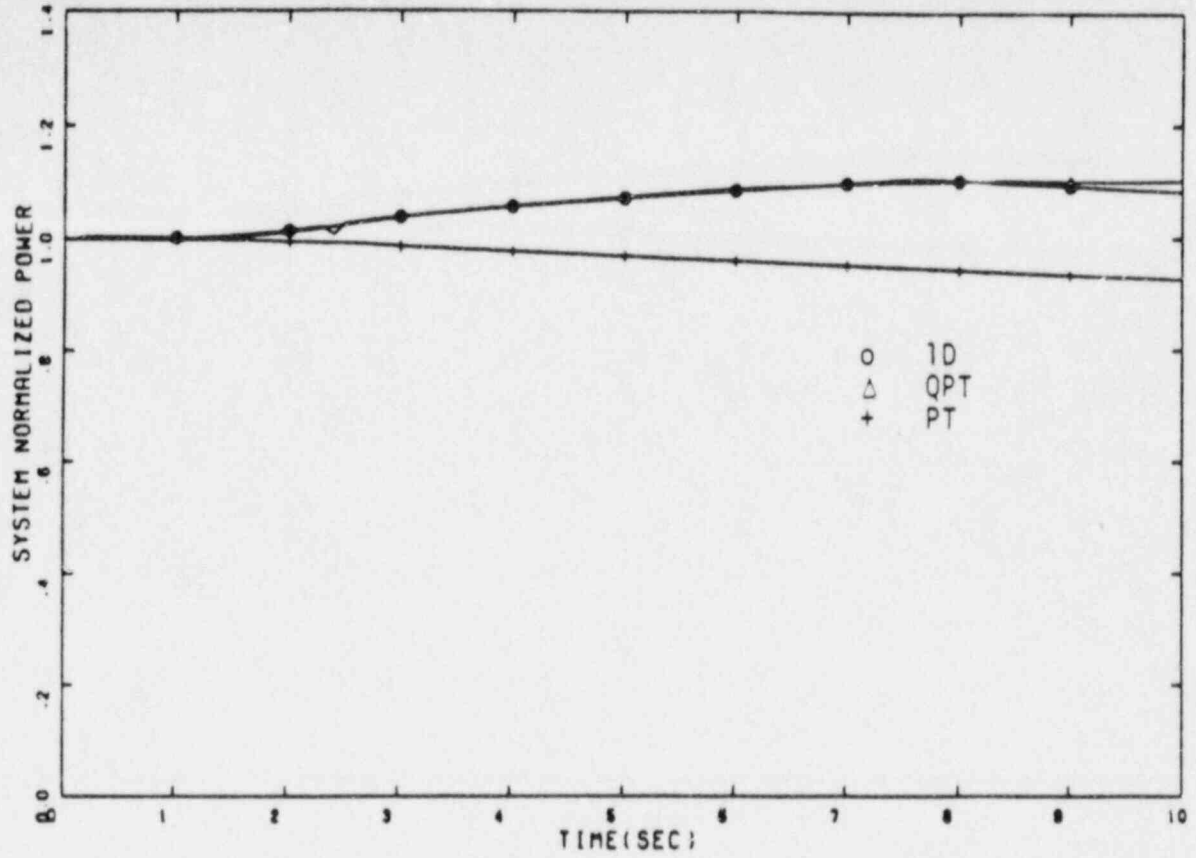

Figure 33 (a) Comparison of System Normalized Power Dur i ng ATWS (LOF) (RETRAN-N)

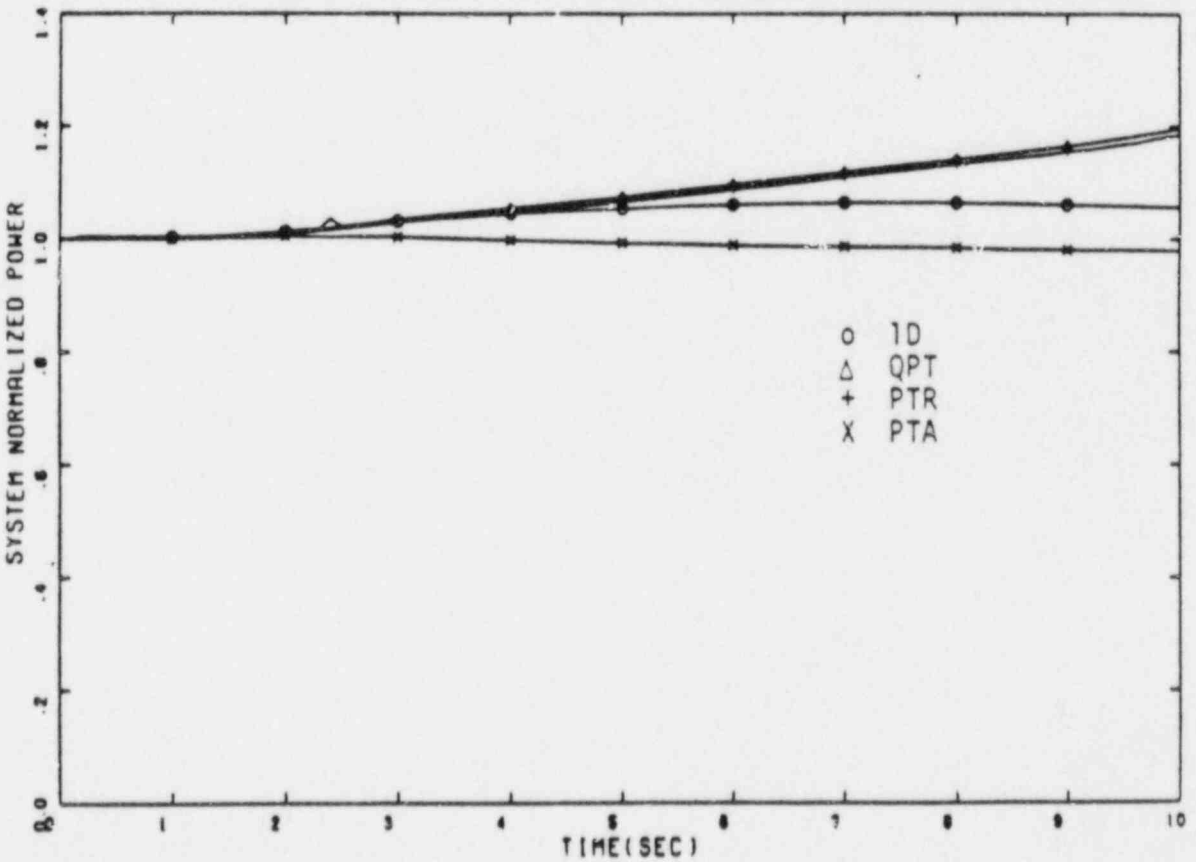

Figure 33 (b) Comparison of System Normalized Power During ATWS (LOF) (RETRAN-S)

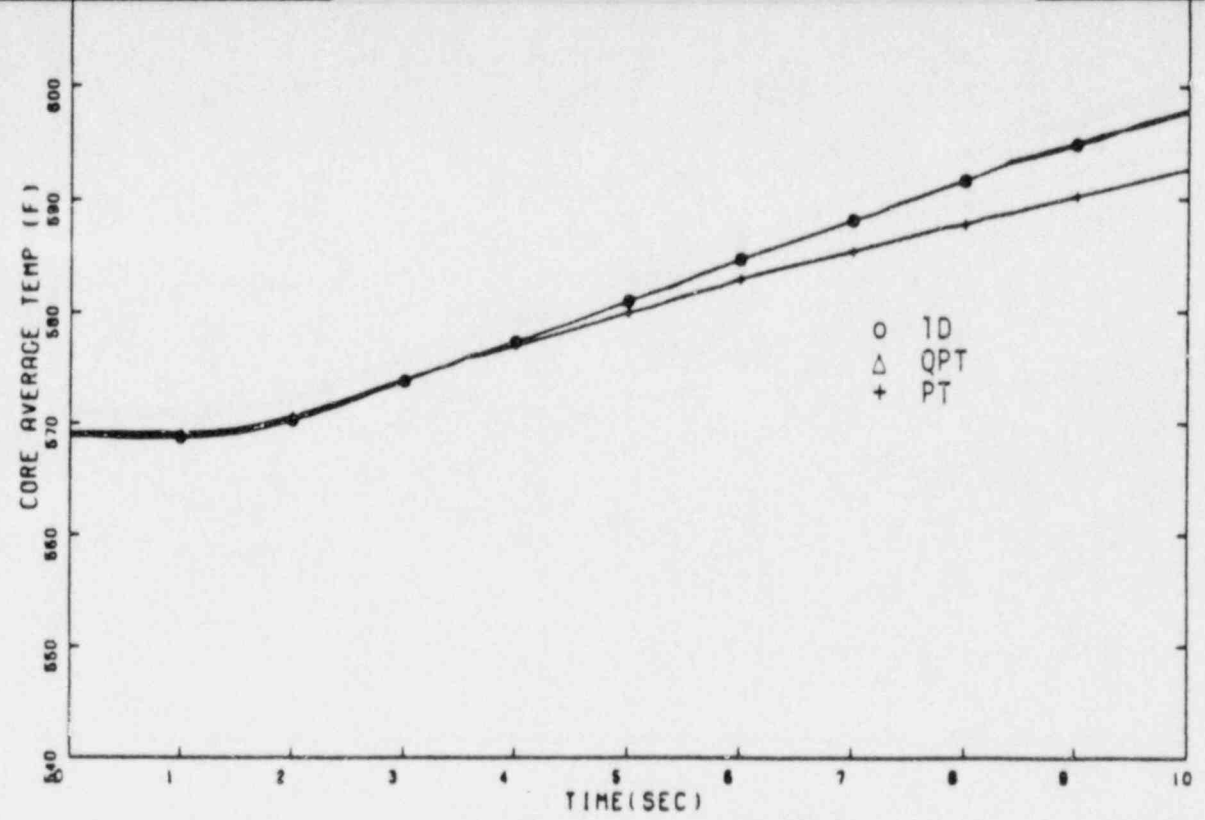

Figure 34 (a) Comparison of Core Average Temperature During ATWS (LOF) (RETRAN-N)

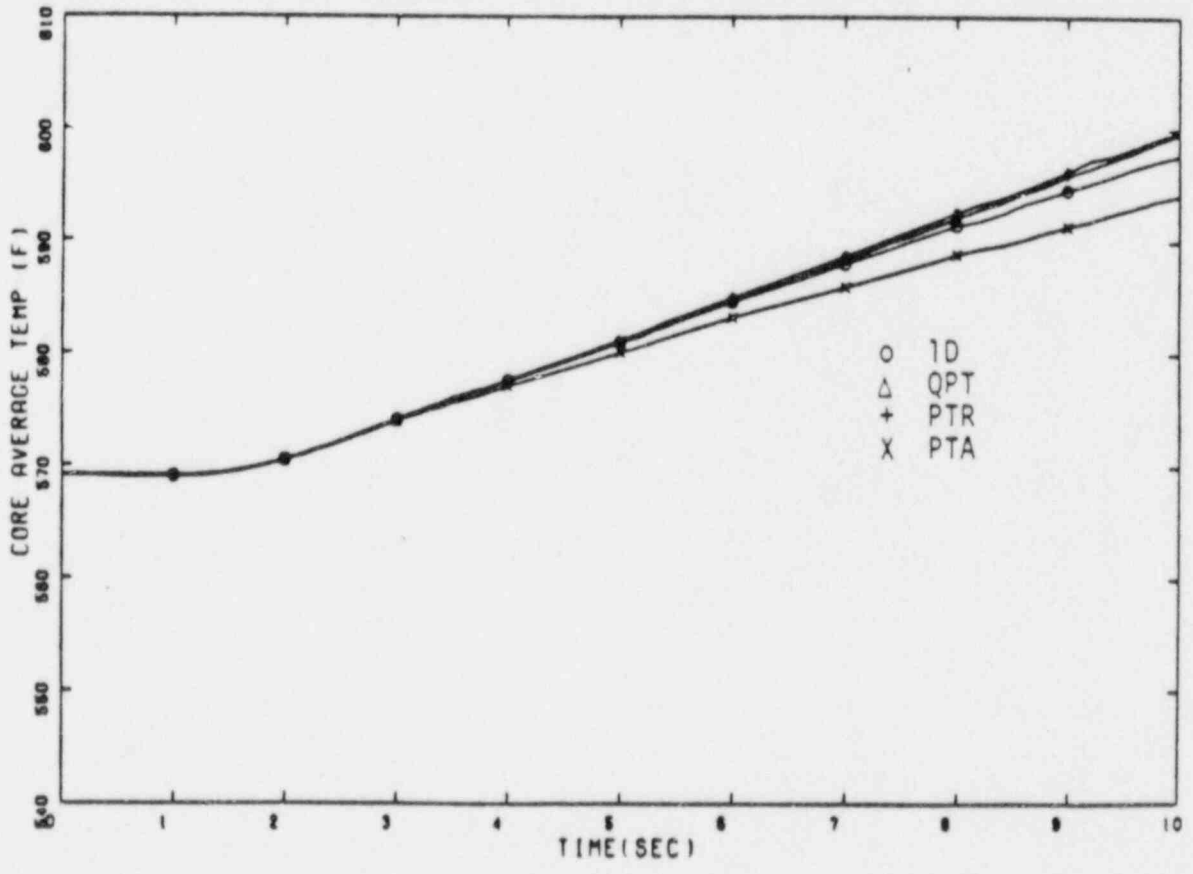

Figure 34 (b) Comparison of Core Average Temperature During ATWS (LOF) (RETRAN-S)

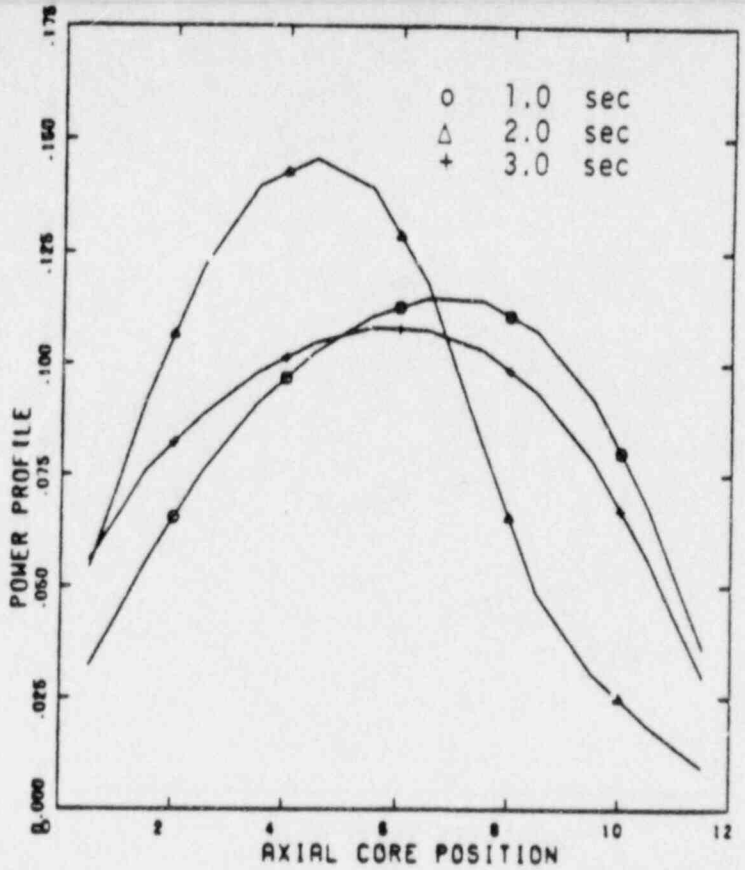

Figure 35 (a) Axial Power Profiles During Scram (RETRAN-N)

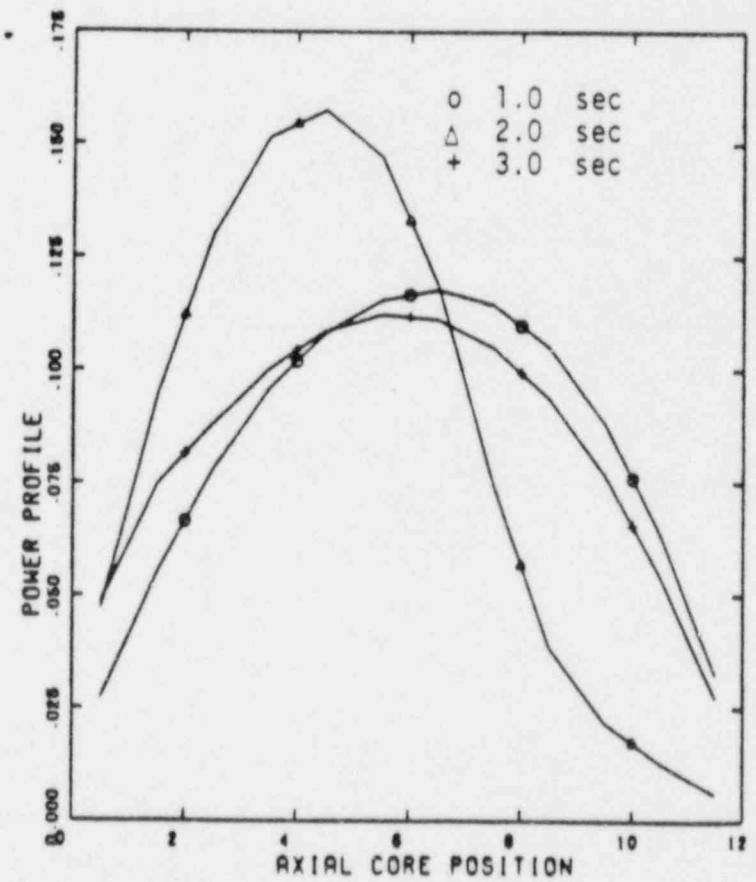

Figure 35 (b) Axial Power Profiles During Scram (RETRAN-S)

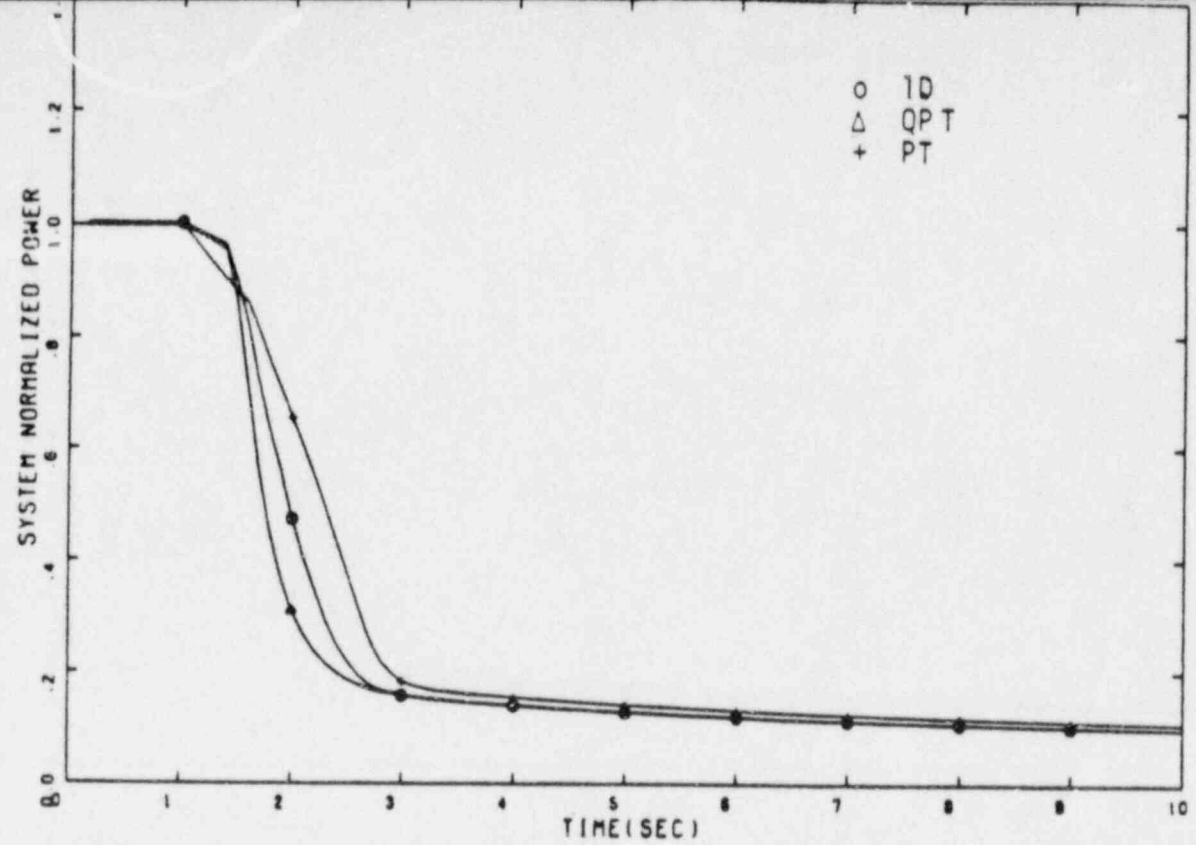

Figure 36 (a) Comparison of System Normalized Power During Scram (RETRAN-N)

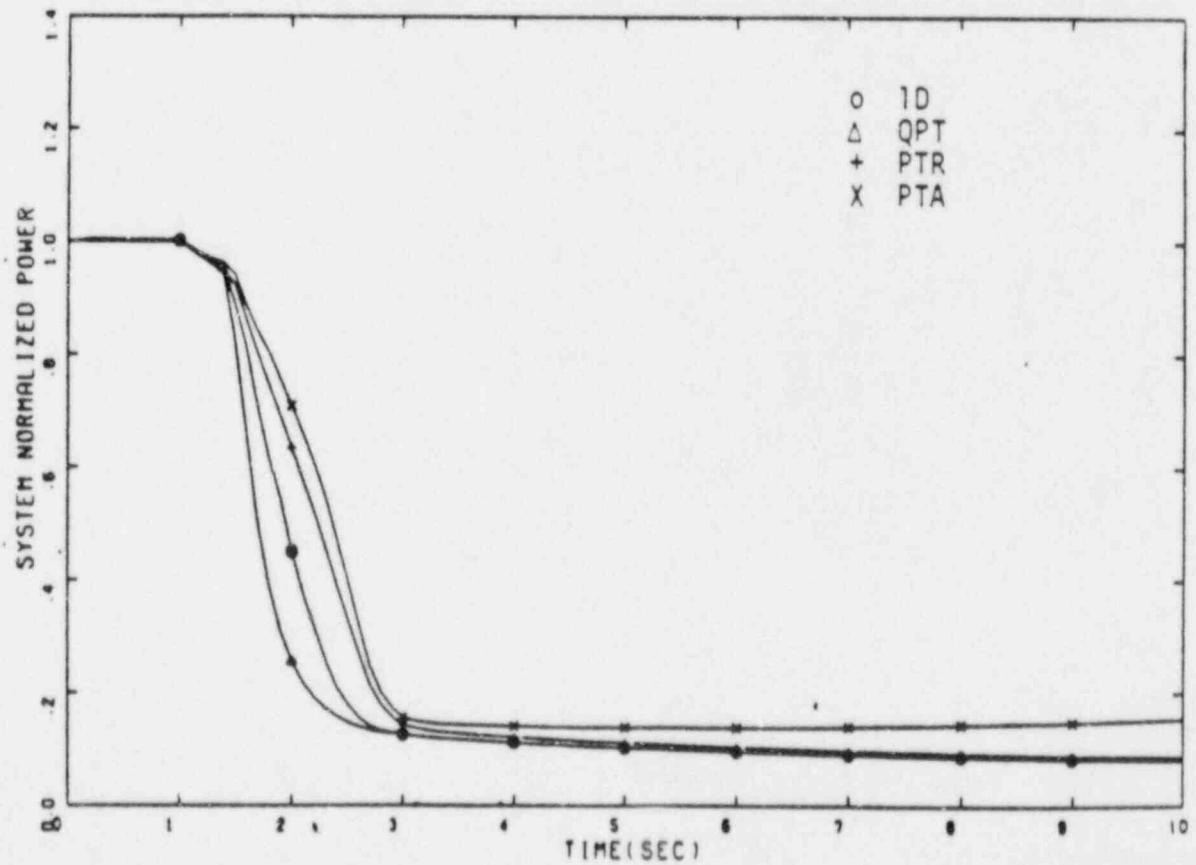

Figure 36 (b) Comparison of System Normalized Power During Scram (RETRAN-S)

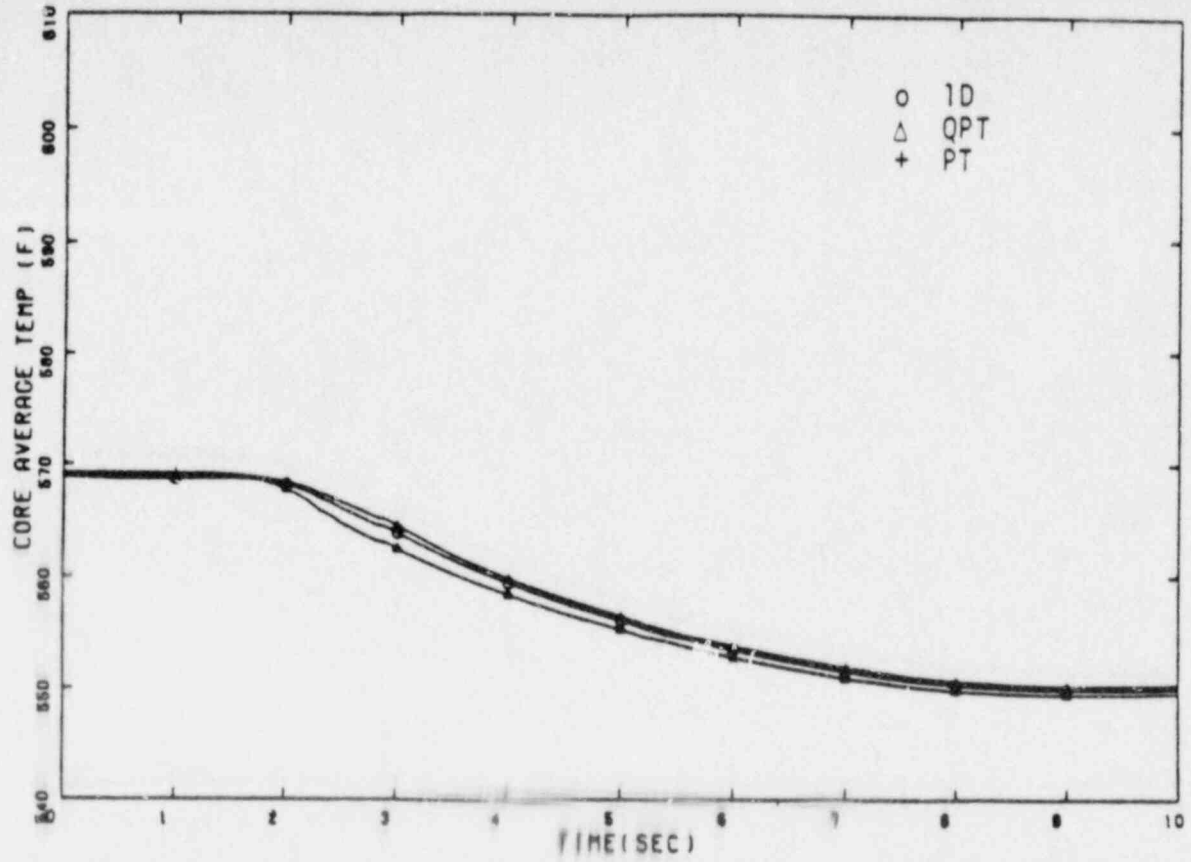

Figure 37 (a) Comparison of Core Average Temperature During Scram (RETRAN-N)

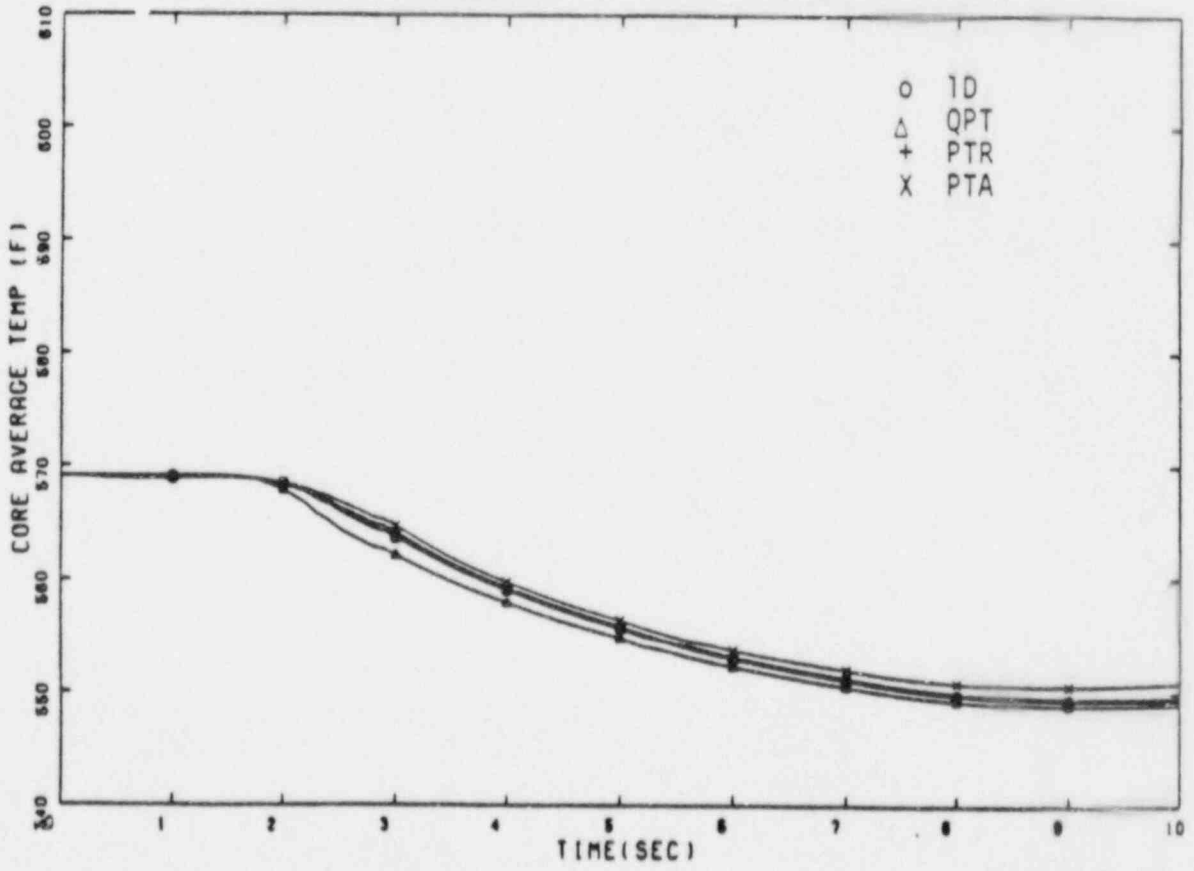

Figure 37 (b) Comparison of Core Average Temperature During Scram (RETRAN-S)

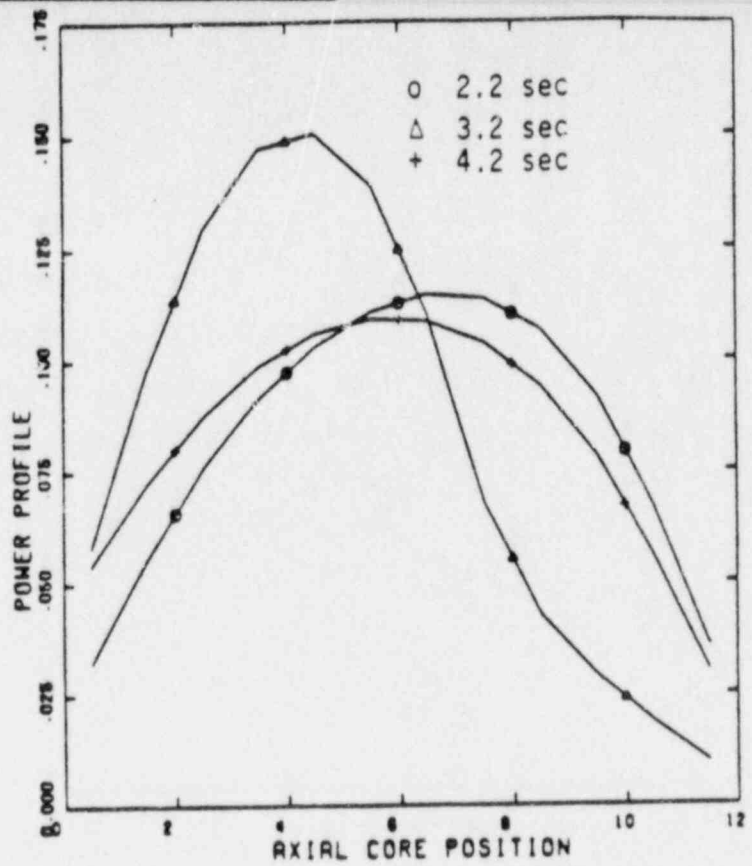

Figure 38 (a) Axial Power Profiles During LOF (RETRAN-N)

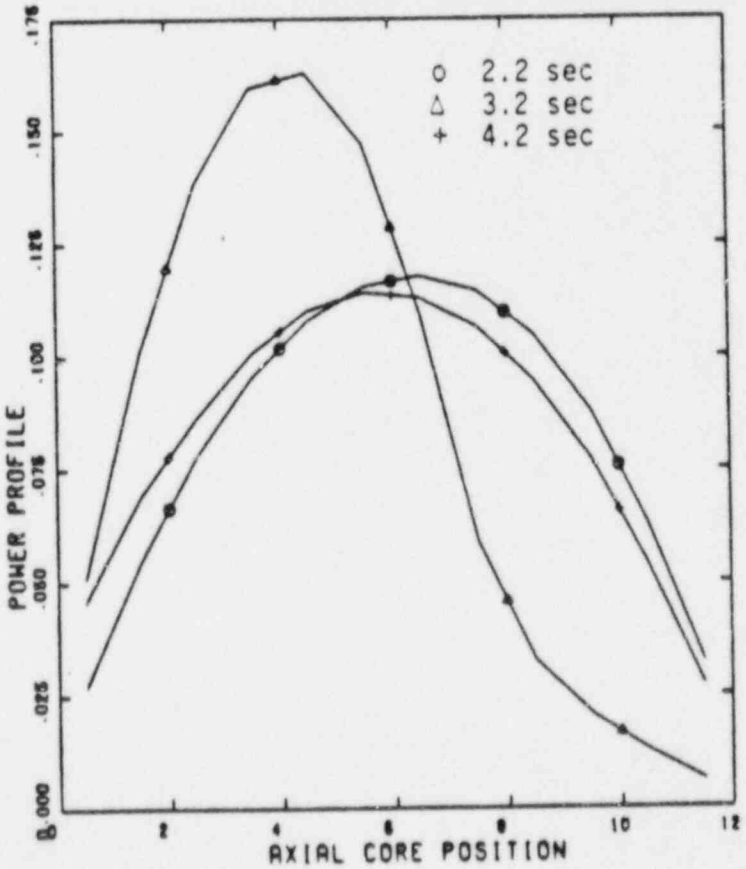

Figure 38 (b) Axial Power Profiles During LOF (RETRAN-S)

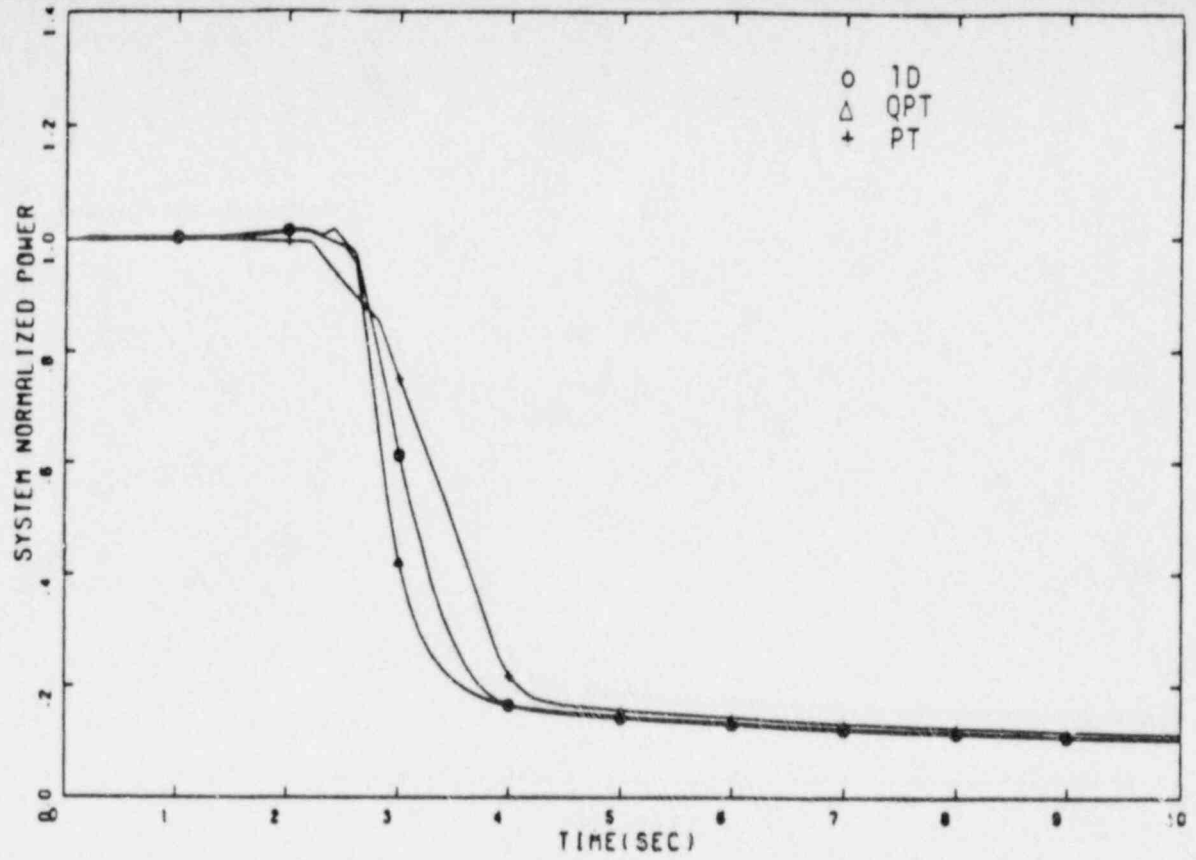

Figure 39 (a) Comparison of System Normalized Power During LOF (RETRAN-N)

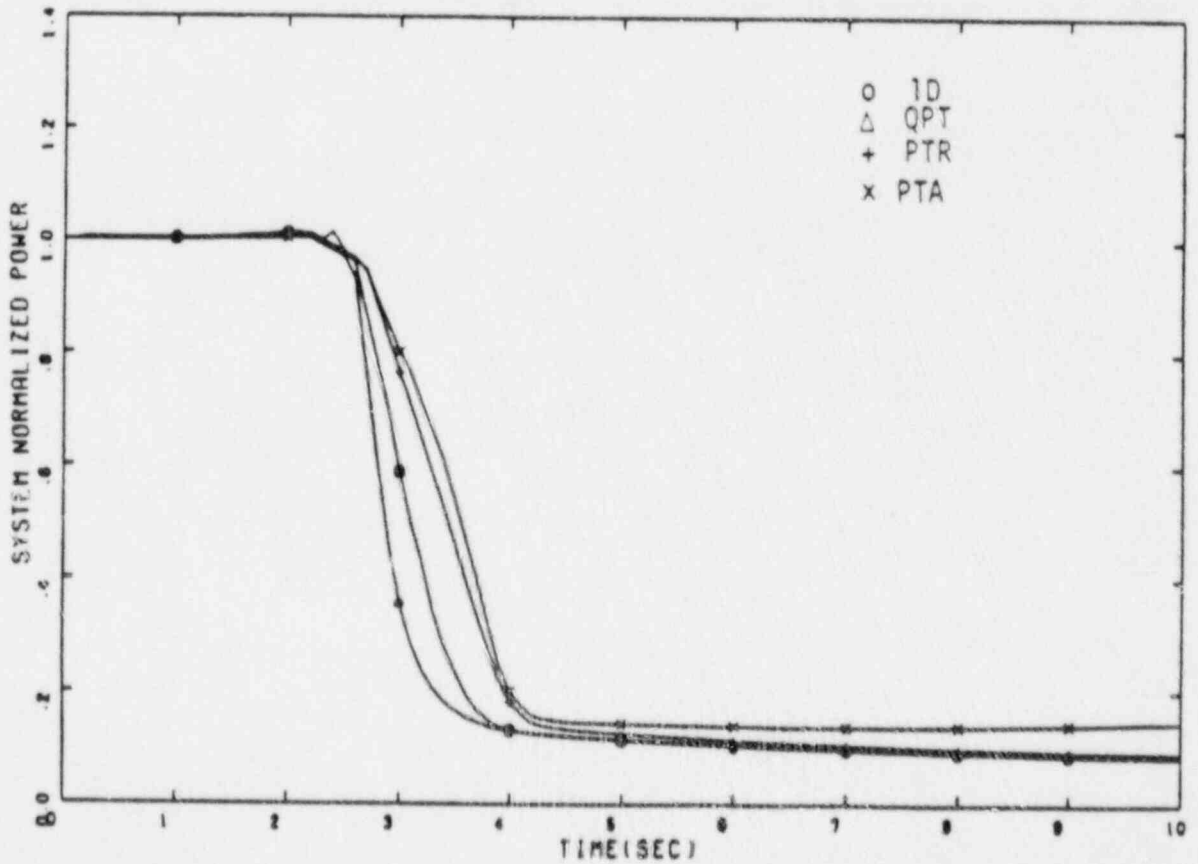

Figure 39 (b) Comparison of System Normalized Power During LOF (RETRAN-S)

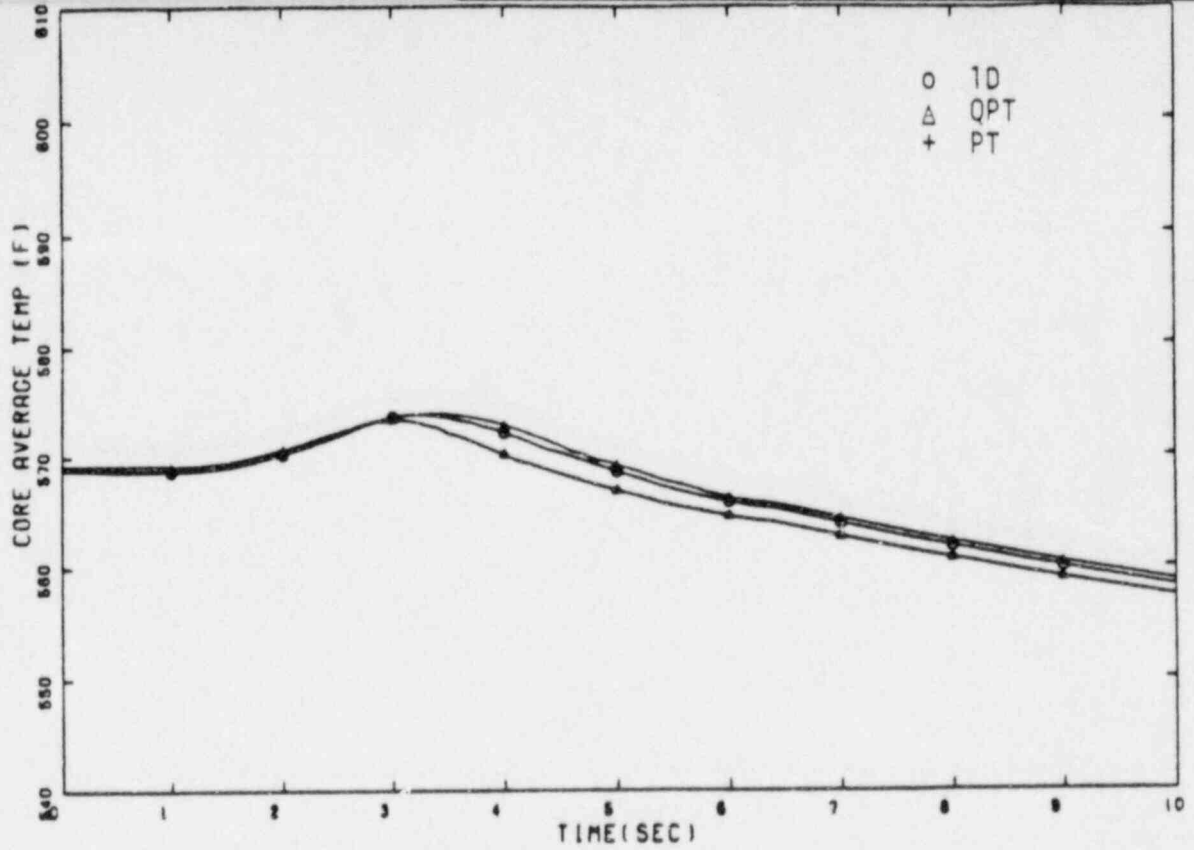

Figure 40 (a) Comparison of Core Average Temperature During LOG

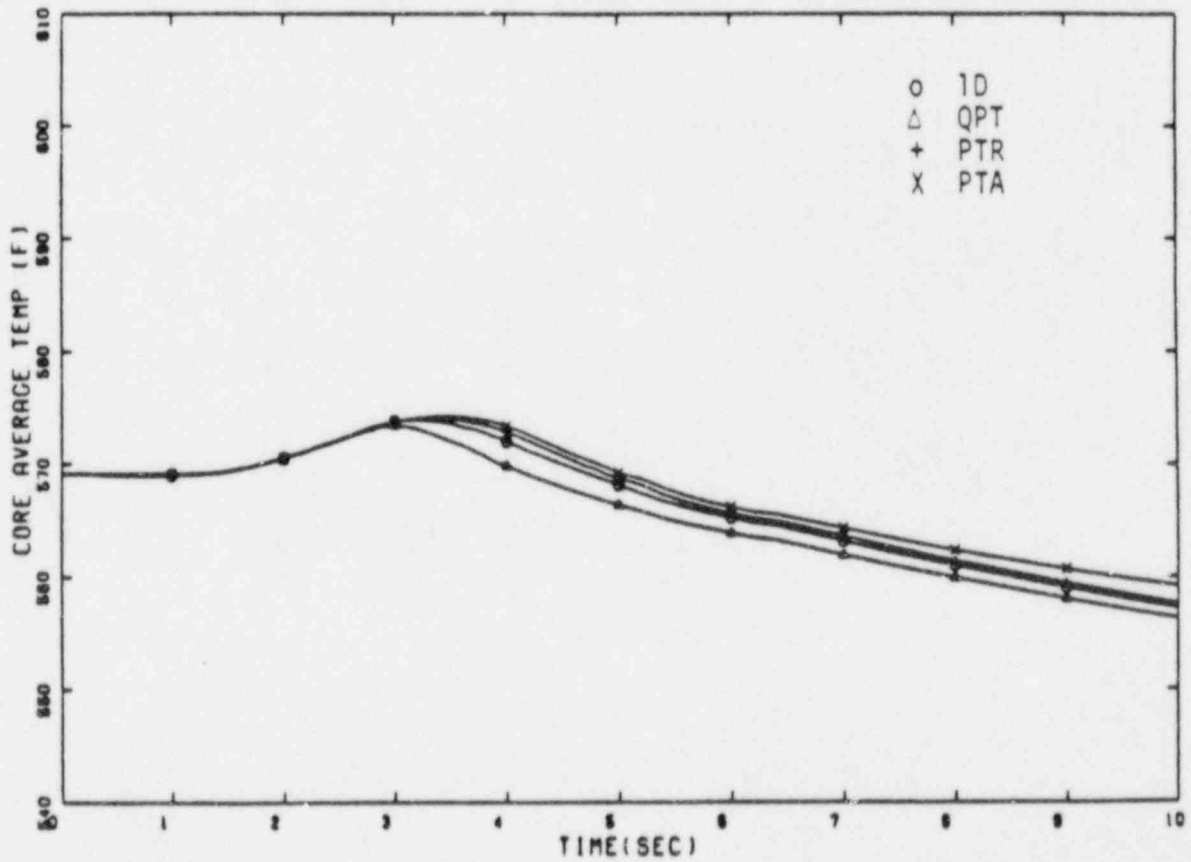

Figure 40 (b) Comparison of Core Average Temperature During LOF